Figures and figure supplements

Molecular consequences of peripheral Influenza A infection on cell populations in the murine hypothalamus

René Lemcke *et al.*

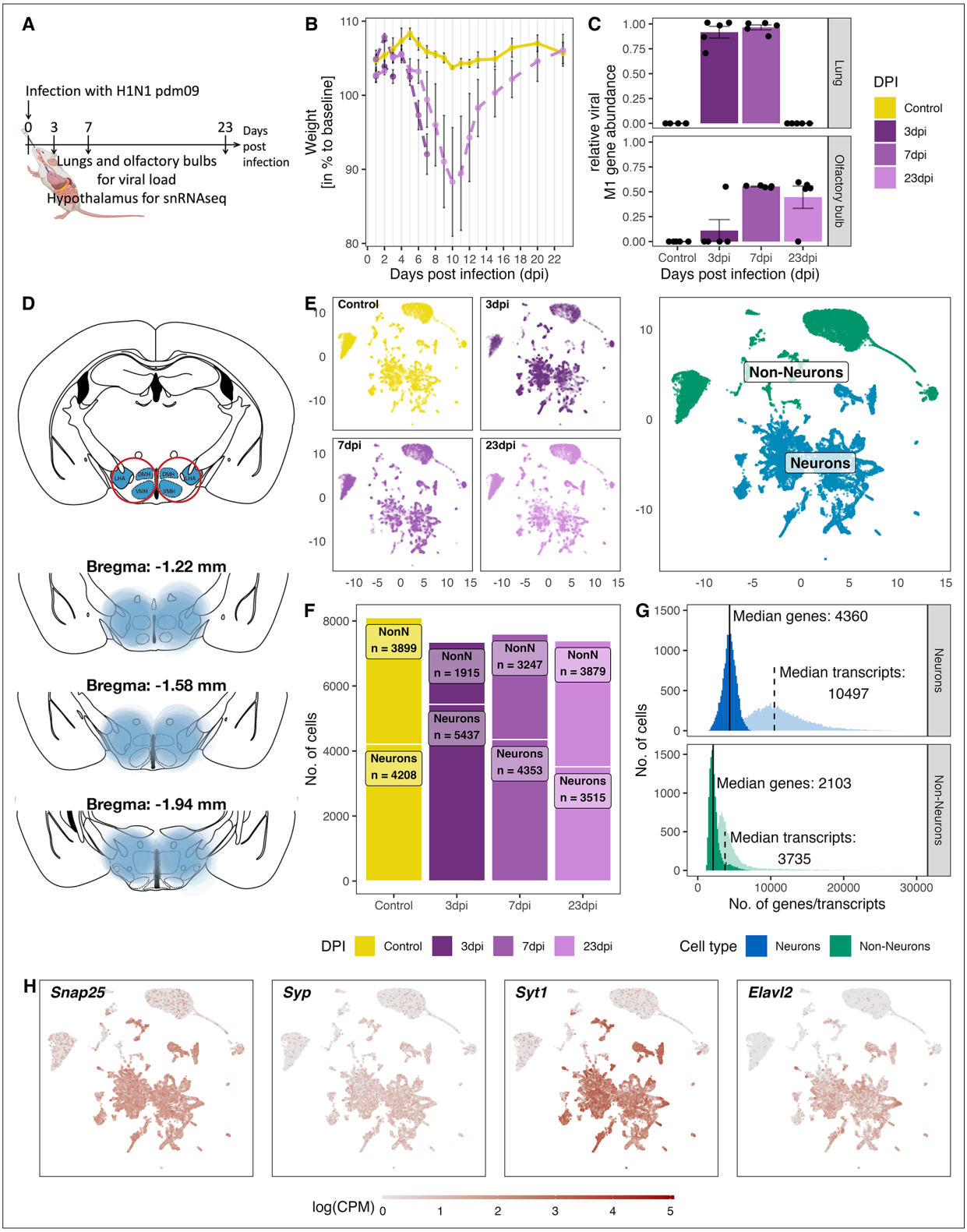

Figure 1. Overview of the experiment, development of the infection, and the resulting snRNA-seq dataset. (**A**) Schematic representation of the experiment. (**B**) Loss of body weight of mice during disease progression until full recovery (n=5 per group). (**C**) Viral M1 gene abundance in lung and olfactory bulb tissue at the three time points during disease progression and in controls. (**D**) Location of microdissection punches of the hypothalamus mapped to the mouse brain atlas at distances from bregma of −1.22, −1.58 and −1.94. (**E**) UMAP dimensional reduction of 30.452 cells, color-coded based on their sample group (different time points and control) membership (left) or their neuronal and non-neuronal identity (right). (**F**) Bar graph

Figure 1 continued on next page

Figure 1 continued

showing the cell counts of neuronal and non-neuronal cells in the different sampling groups. (**G**) Histograms depicting the distribution of transcript (lighter shading) and genes (solid shading) in all non-neuronal and neuronal cells. (**H**) Normalized expression of neuronal marker genes (*Snap25*, *Syp*, *Syt1*, *Elval2*) in all cells shown on a UMAP plot.

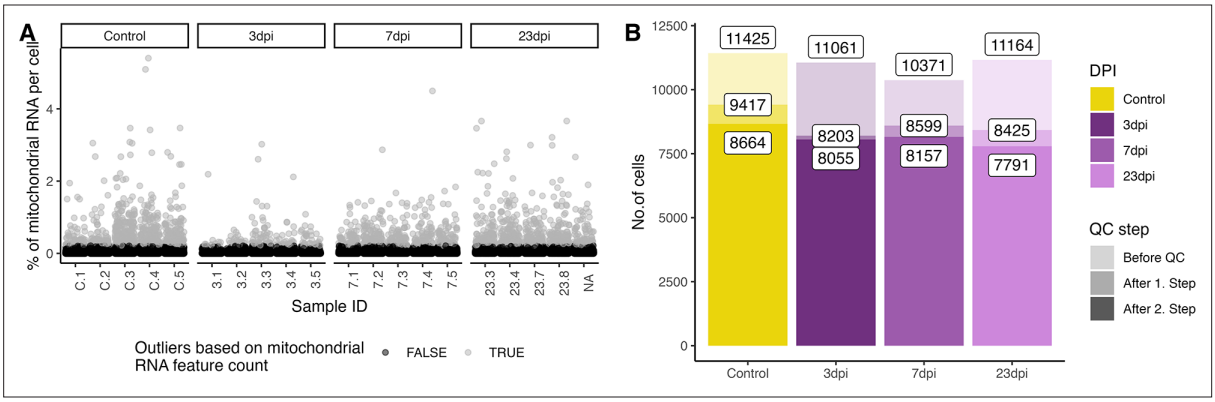

Figure 1—figure supplement 1. Quality control plots for the generated snRNA-seq dataset. (**A**) Percentages of mitochondrial RNA in the different samples. Light gray dots were categorised as outliers and removed form the downstream analysis. (**B**) Cell counts per time point after different filter steps.

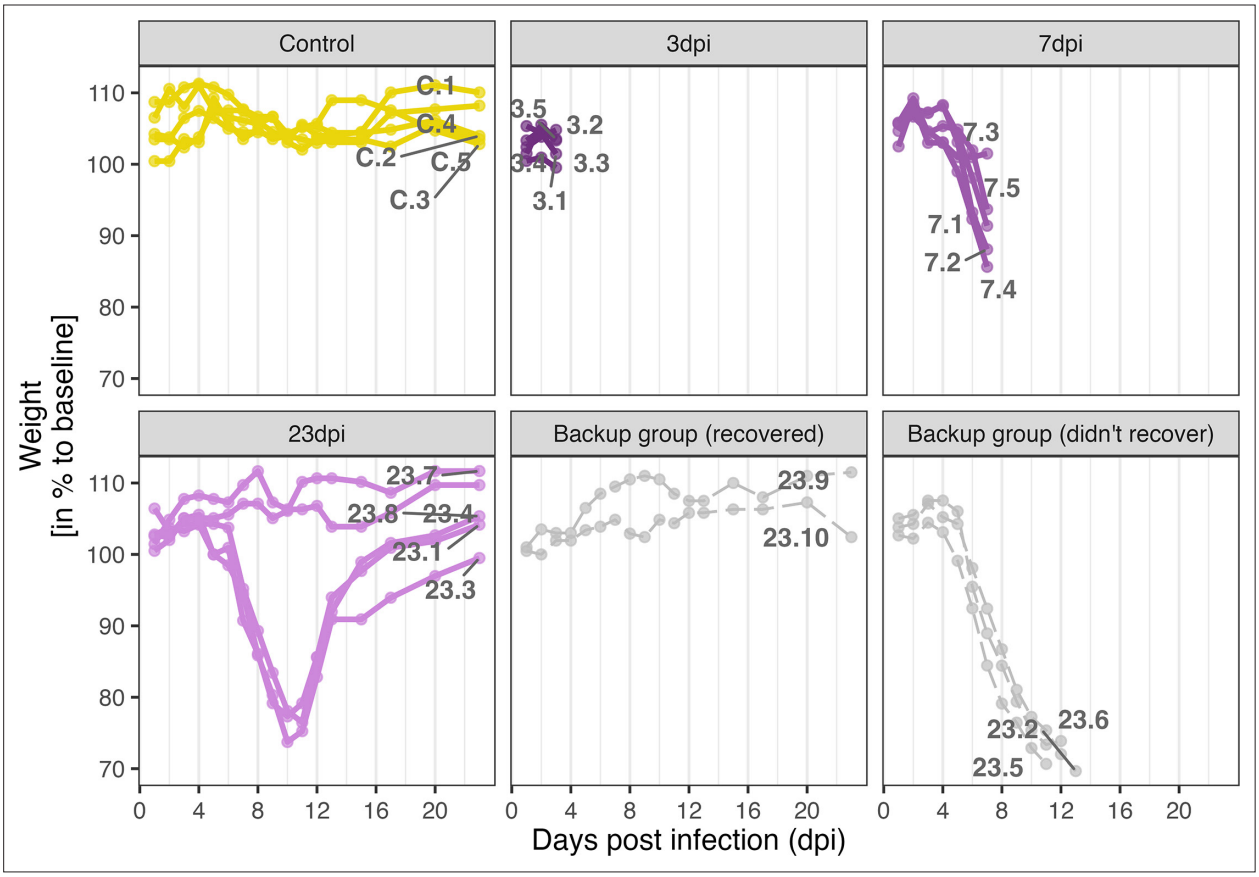

Figure 1—figure supplement 2. Weight curves depicting the weight-loss due to H1N1 pdm09 infection in the different individuals. Weight curves are group by time point samples. Grey coloured animals were not used for snRNA-sequencing.

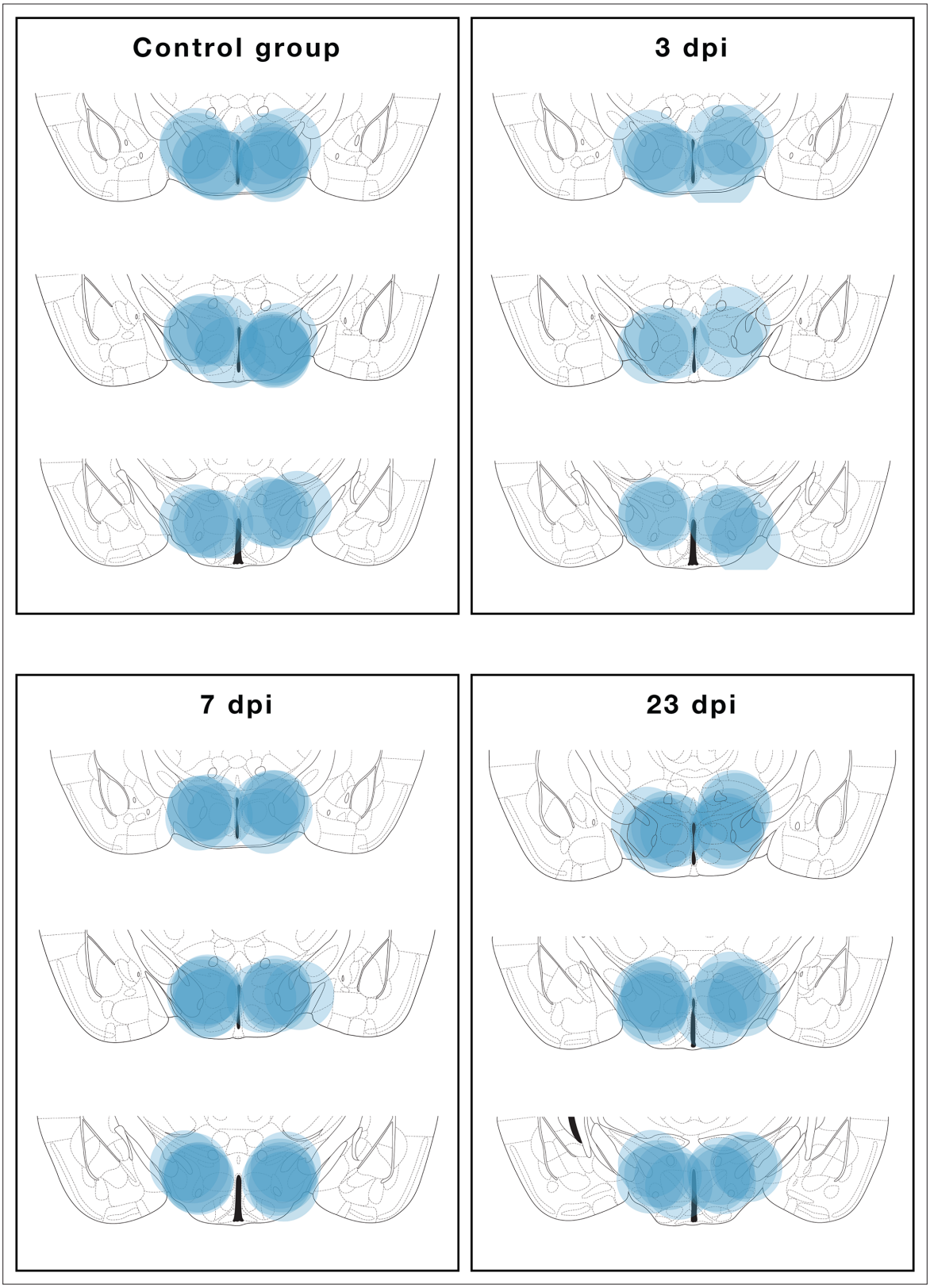

Figure 1—figure supplement 3. Punching location. Location of 4 mm punches for RNA extraction and snRNA-seq in the hypothalamus in the different sampling groups.

Figure 1—figure supplement 4. UMAP embeddings per hash-tagged sample. UMAP embeddings show the distribution of cells across the different cell types of the individual hash-tagged samples. Colours depict and shadings depict the time points.

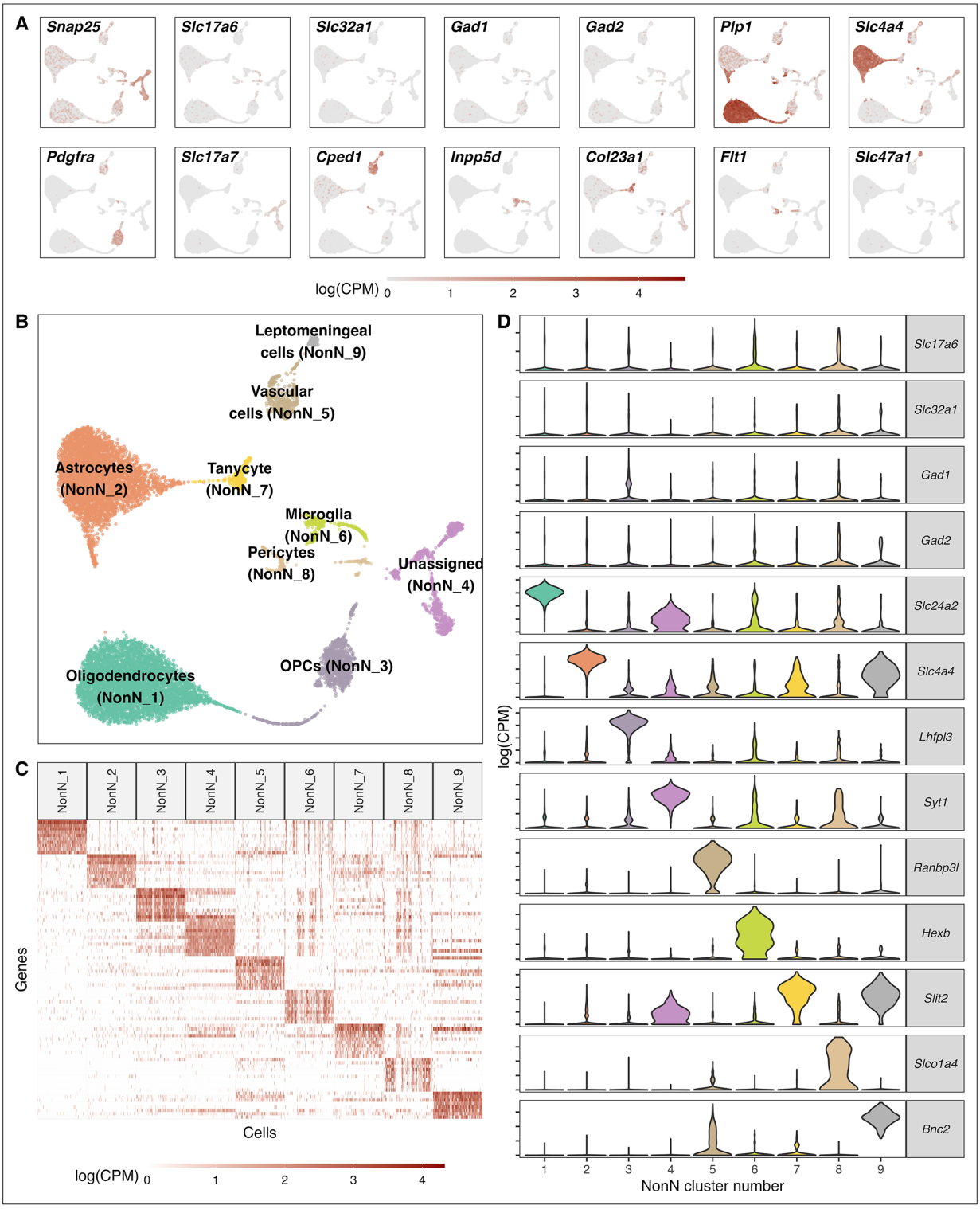

Figure 2. Classification of non-neuronal cell types. (**A**) Normalized expression values of different neuronal and non-neuronal cell type markers (pan-neuronal marker - *Snap25*; Glutamatergic marker - *Slc17a6*; GABAergic markers - *Slc32a1*, *Gad1*, *Gad2*; Oligodendrocyte marker – *Plp1*; Astrocyte markers – *Slc4a4*; Oligodendrocyte precursor marker – *Pdgfra; Cped1* – Vascular and leptomeningeal cell markers – *Cped1*, *Slc47a1*, Microglia marker – *Inpp5d*, Tanycytic marker – *Col23a1*, Pericyte marker – *Flt1*) in all non-neuronal cells (n=12.940) mapped on a UMAP. (**B**) Unsupervised clustering of non-neuronal cell types shown in a UMAP embedding and color-coded and annotated by potential cell type annotations. (**C**) Heatmap of normalized expression values showing discriminatory cell type markers of 9 non-neuronal cell populations. (**D**) Violin plots showing distribution of normalized expression values of neurotransmitters and best discriminatory cell type markers.

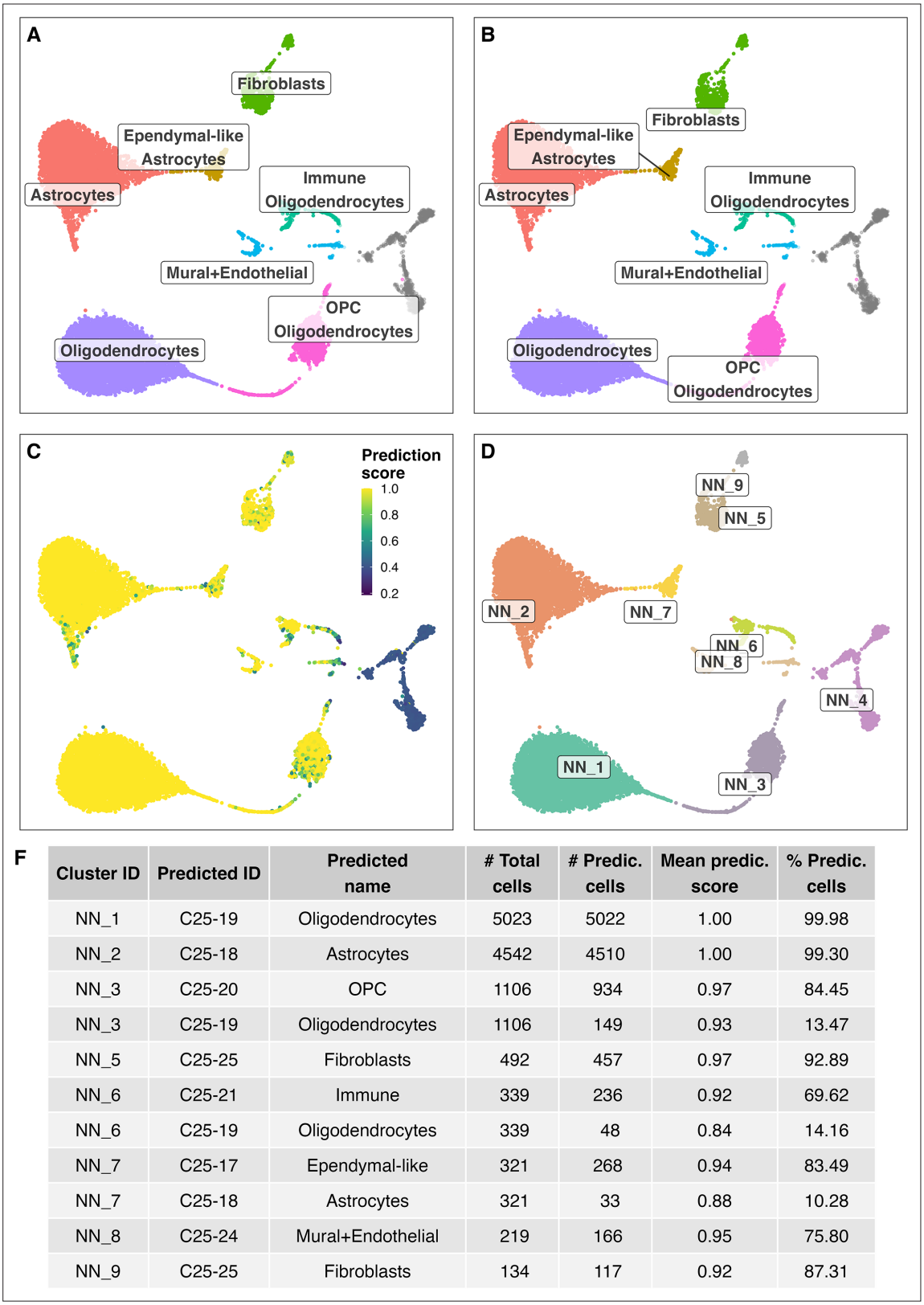

F

Cluster ID	Predicted ID	Predicted name	# Total cells	# Predic. cells	Mean predic. score	% Predic. cells
NN_1	C25-19	Oligodendrocytes	5023	5022	1.00	99.98
NN_2	C25-18	Astrocytes	4542	4510	1.00	99.30
NN_3	C25-20	OPC	1106	934	0.97	84.45
NN_3	C25-19	Oligodendrocytes	1106	149	0.93	13.47
NN_5	C25-25	Fibroblasts	492	457	0.97	92.89
NN_6	C25-21	Immune	339	236	0.92	69.62
NN_6	C25-19	Oligodendrocytes	339	48	0.84	14.16
NN_7	C25-17	Ependymal-like	321	268	0.94	83.49
NN_7	C25-18	Astrocytes	321	33	0.88	10.28
NN_8	C25-24	Mural+Endothelial	219	166	0.95	75.80
NN_9	C25-25	Fibroblasts	134	117	0.92	87.31

Figure 2—figure supplement 1. Label transfer of cell-type labels from the HypoMap (***Steuernagel et al., 2022***) annotations (C7) to the Non-neuronal cell cluster here identified. (**A/B**) Shows the cell label transfer for HypoMap cell-type level C7. (**C**) Depicts prediction scores. (**D**) Original cell-clusters and labels identified in the here presented study. (**F**) Detailed overview of predicted names for the different identified cell clusters.

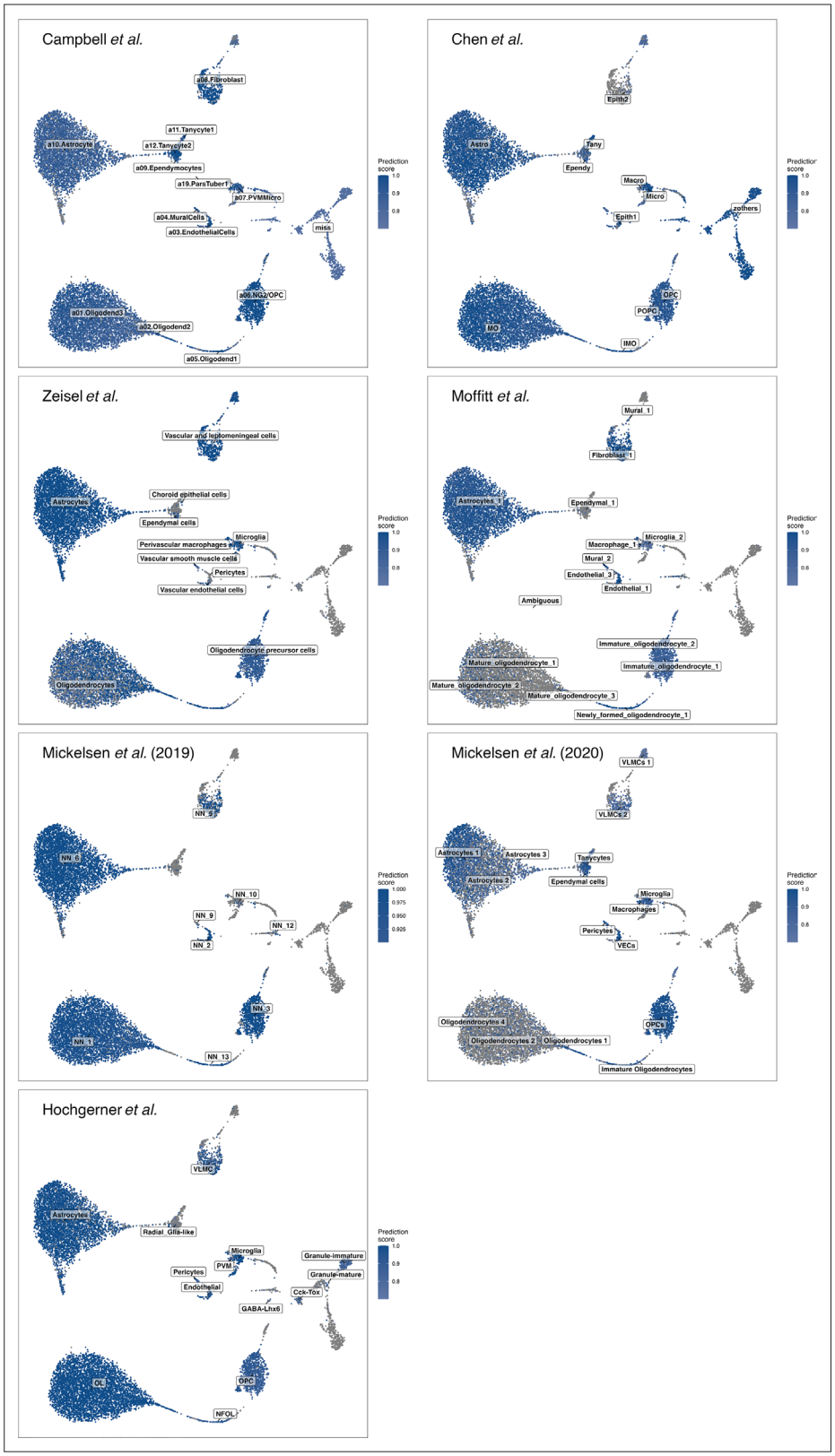

Figure 2—figure supplement 2. Cell-type label transfer for non-neuronal cells. Depicting the prediction scores and potential cell-type labels in non-neuronal cells from different published datasets (***Campbell et al., 2017***; ***Chen et al., 2017***; ***Hochgerner et al., 2018***; ***Mickelsen et al., 2019***; ***Mickelsen et al., 2020***; ***Moffitt et al., 2018***; ***Zeisel et al., 2018***).

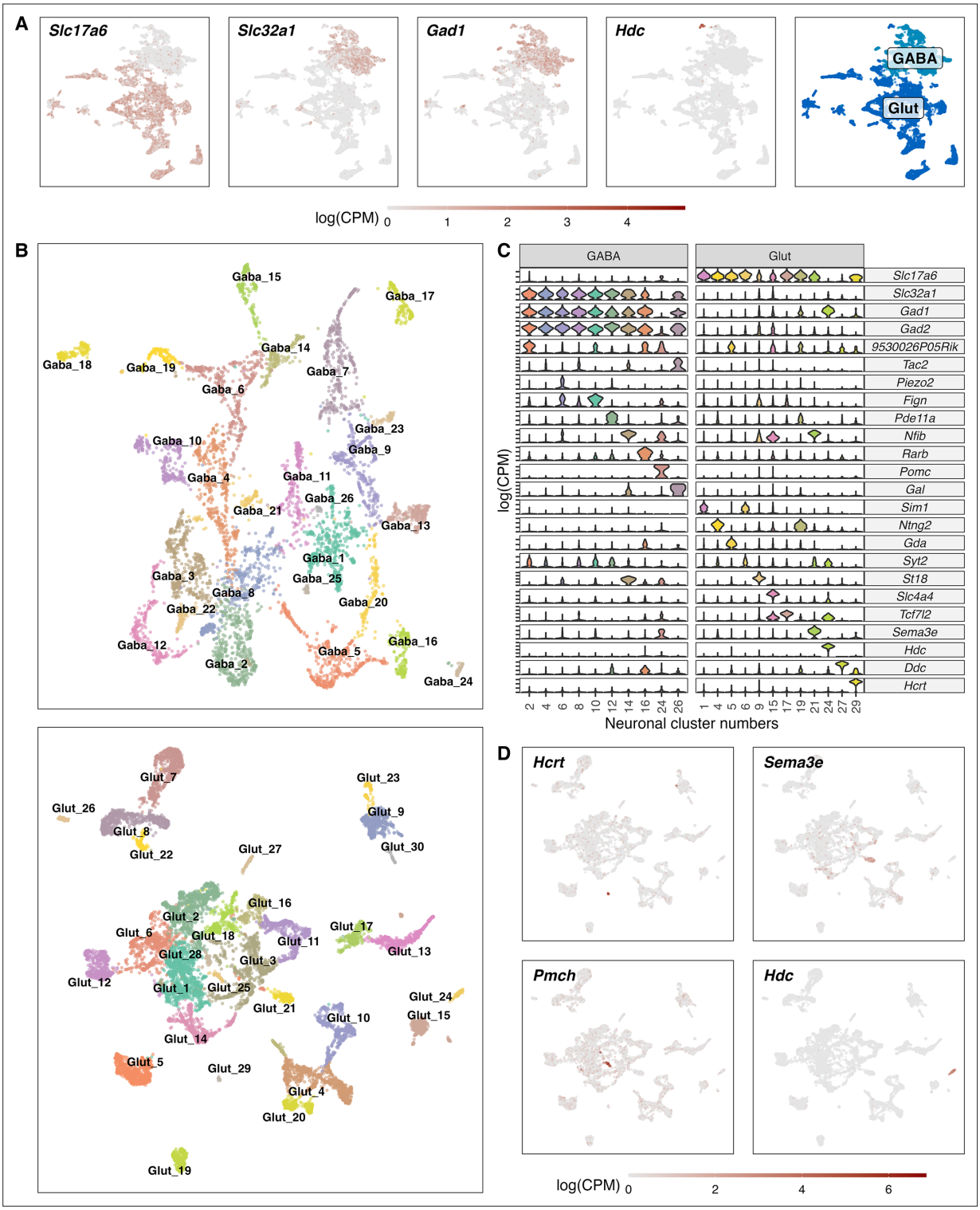

Figure 3. Classification of GABAergic and glutamatergic neuronal cell types in the hypothalamus. (**A**) Normalized expression values of different neurotransmitters (Glutamatergic marker - Slc17a6; GABAergic markers - *Slc32a1*, *Gad1*, *Gad2*) in all neuronal cells (left) and a color-coded UMAP projection based on their GABAergic or glutamatergic identity (right) (n=17.512). (**B**) Un-supervised clustering of GABAergic (upper, n=6.032) and glutamatergic (lower, n=11.481) cells in UMAP plots. Cell type clusters are color-coded and annotated with labels. (**C**) Violin plots showing normalized expression values of neurotransmitters and discriminating marker genes of selected GABAergic (left) and glutamatergic (right) cell type clusters. (**D**) Glutamatergic UMAP plots showing normalized expression values of distinct markers for hypothalamic neuron populations (HCRT neurons – upper left, PMCH neurons – lower left, GnRH neurons – upper right, Histaminergic neurons – lower right).

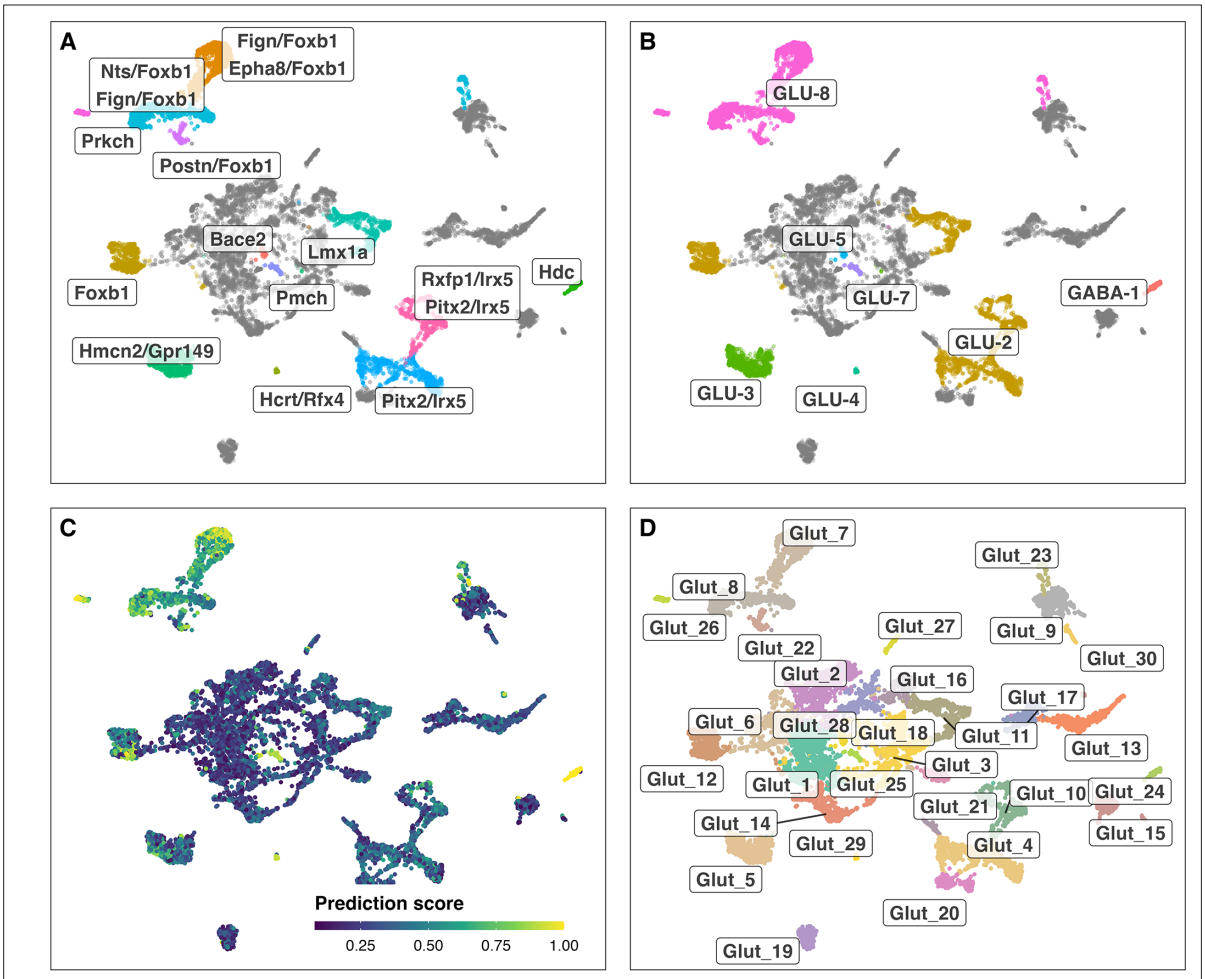

F

Cluster ID	Predicted ID	Predicted name	Predic. Cell ID	Markers	# Total cells	# Predic. cells	Mean predic. score	% Predic. cells
Glut_10	C185-6	Rxfp1.Irx5.GLU-2	GLU-2	Rxfp1/Irx5	520	73	0.62	14.04
Glut_10	C185-4	Pitx2.Irx5.GLU-2	GLU-2	Pitx2/Irx5	520	62	0.58	11.92
Glut_11	C185-20	Lmx1a.GLU-2	GLU-2	Lmx1a	476	83	0.56	17.44
Glut_12	C185-19	Foxb1.GLU-2	GLU-2	Foxb1	476	241	0.78	50.63
Glut_22	C185-58	Postn.Foxb1.GLU-8	GLU-8	Postn/Foxb1	100	43	0.75	43.00
Glut_23	C185-57	Nts.Foxb1.GLU-8	GLU-8	Nts/Foxb1	98	30	0.68	30.61
Glut_23	C185-59	Fign.Foxb1.GLU-8	GLU-8	Fign/Foxb1	98	27	0.71	27.55
Glut_24	C185-102	Hdc.GABA-1	GABA-1	Hdc	94	91	0.99	96.81
Glut_25	C185-56	Pmch.GLU-7	GLU-7	Pmch	85	80	0.86	94.12
Glut_26	C185-61	Prkch.GLU-8	GLU-8	Prkch	80	76	0.93	95.00
Glut_28	C185-52	Bace2.GLU-5	GLU-5	Bace2	64	26	0.64	40.62
Glut_29	C185-47	Hcrt.Rfx4.GLU-4	GLU-4	Hcrt/Rfx4	38	35	0.92	92.11
Glut_4	C185-4	Pitx2.Irx5.GLU-2	GLU-2	Pitx2/Irx5	744	84	0.57	11.29
Glut_5	C185-30	Hmcn2.Gpr149.GLU-3	GLU-3	Hmcn2/Gpr149	694	148	0.67	21.33
Glut_7	C185-59	Fign.Foxb1.GLU-8	GLU-8	Fign/Foxb1	625	386	0.81	61.76
Glut_7	C185-60	Epha8.Foxb1.GLU-8	GLU-8	Epha8/Foxb1	625	164	0.65	26.24
Glut_8	C185-57	Nts.Foxb1.GLU-8	GLU-8	Nts/Foxb1	604	305	0.71	50.50
Glut_8	C185-59	Fign.Foxb1.GLU-8	GLU-8	Fign/Foxb1	604	75	0.63	12.42

Figure 3—figure supplement 1. Label transfer of cell-type labels from the HypoMap (***Steuernagel et al., 2022***) annotations (C285) to glutamatergic cell cluster here identified. (**A/B**) Shows the cell label transfer for HypoMap cell-type level C285 (_named).(**C**) Depicts prediction scores.(**D**) Original cell-clusters and labels identified in the here presented study.(**F**) Detailed overview of predicted names for the different identified cell clusters.

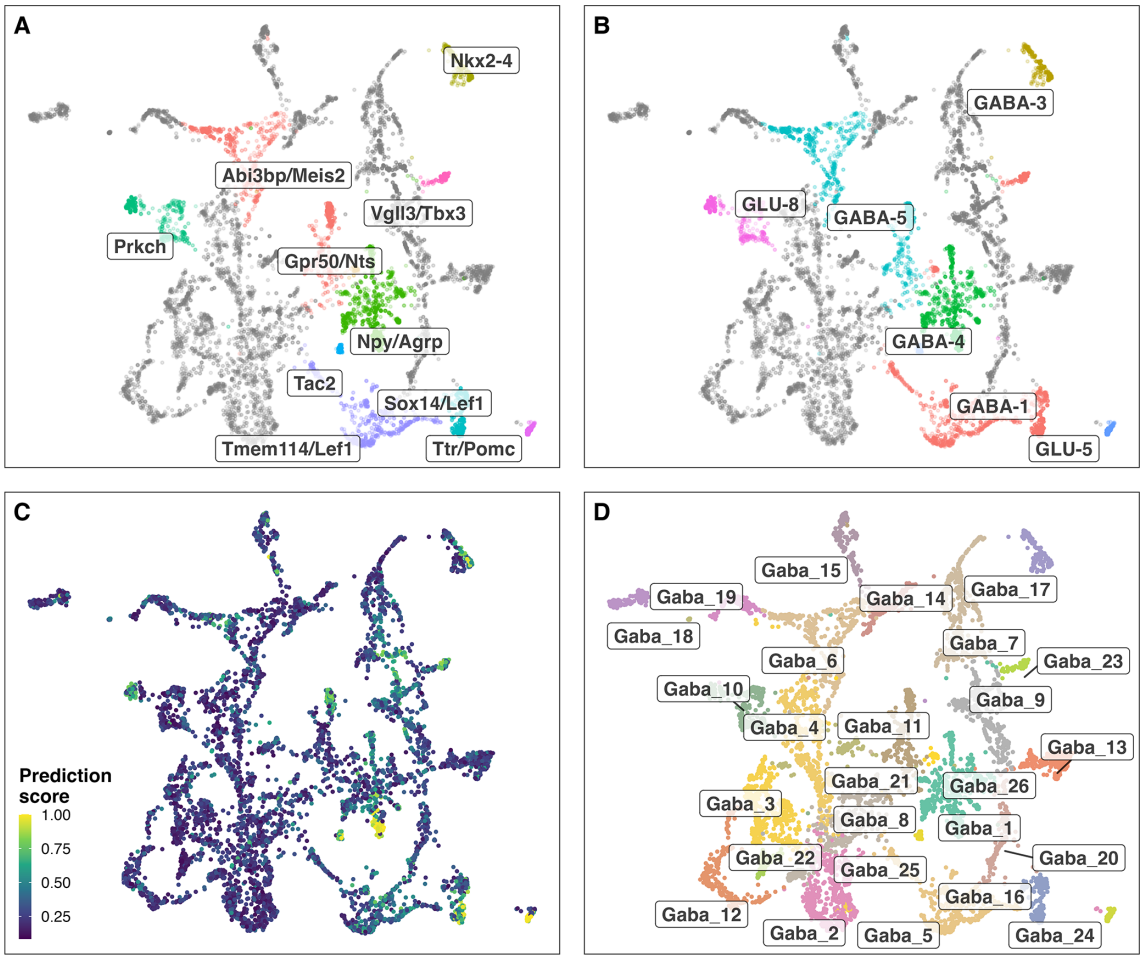

F

Cluster ID	Predicted ID	Predicted name	Predic. Cell ID	Markers	# Total cells	# Predic. cells	Mean predic. score	% Predic. cells
Gaba_1	C185-115	Npy.Agrp.GABA-4	GABA-4	Npy/Agrp	486	64	0.96	13.17
Gaba_10	C185-61	Prkch.GLU-8	GLU-8	Prkch	265	38	0.73	14.34
Gaba_11	C185-121	Abi3bp.Meis2.GABA-5	GABA-5	Abi3bp/Meis2	250	60	0.71	24.00
Gaba_16	C185-88	Sox14.Lef1.GABA-1	GABA-1	Sox14/Lef1	161	76	0.77	47.20
Gaba_17	C185-113	Nkx2-4.GABA-3	GABA-3	Nkx2-4	144	39	0.70	27.08
Gaba_23	C185-103	Vgll3.Tbx3.GABA-1	GABA-1	Vgll3/Tbx3	68	35	0.74	51.47
Gaba_24	C185-50	Ttr.Pomc.GLU-5	GLU-5	Ttr/Pomc	62	36	0.95	58.06
Gaba_25	C185-51	Tac2.GLU-5	GLU-5	Tac2	41	37	0.77	90.24
Gaba_26	C185-110	Gpr50.Nts.GABA-1	GABA-1	Gpr50/Nts	29	8	0.62	27.59
Gaba_5	C185-86	Tmem114.Lef1.GABA-1	GABA-1	Tmem114/Lef1	394	46	0.62	11.68
Gaba_6	C185-121	Abi3bp.Meis2.GABA-5	GABA-5	Abi3bp/Meis2	378	40	0.66	10.58

Figure 3—figure supplement 2. Label transfer of cell-type labels from the HypoMap (***Steuernagel et al., 2022***) annotations (C285) to GABAergic cell cluster here identified. (**A/B**) Shows the cell label transfer for HypoMap cell-type level C285 (_named).(**C**) Depicts prediction scores.(**D**) Original cell-clusters and labels identified in the here presented study.(**F**) Detailed overview of predicted names for the different identified cell clusters.

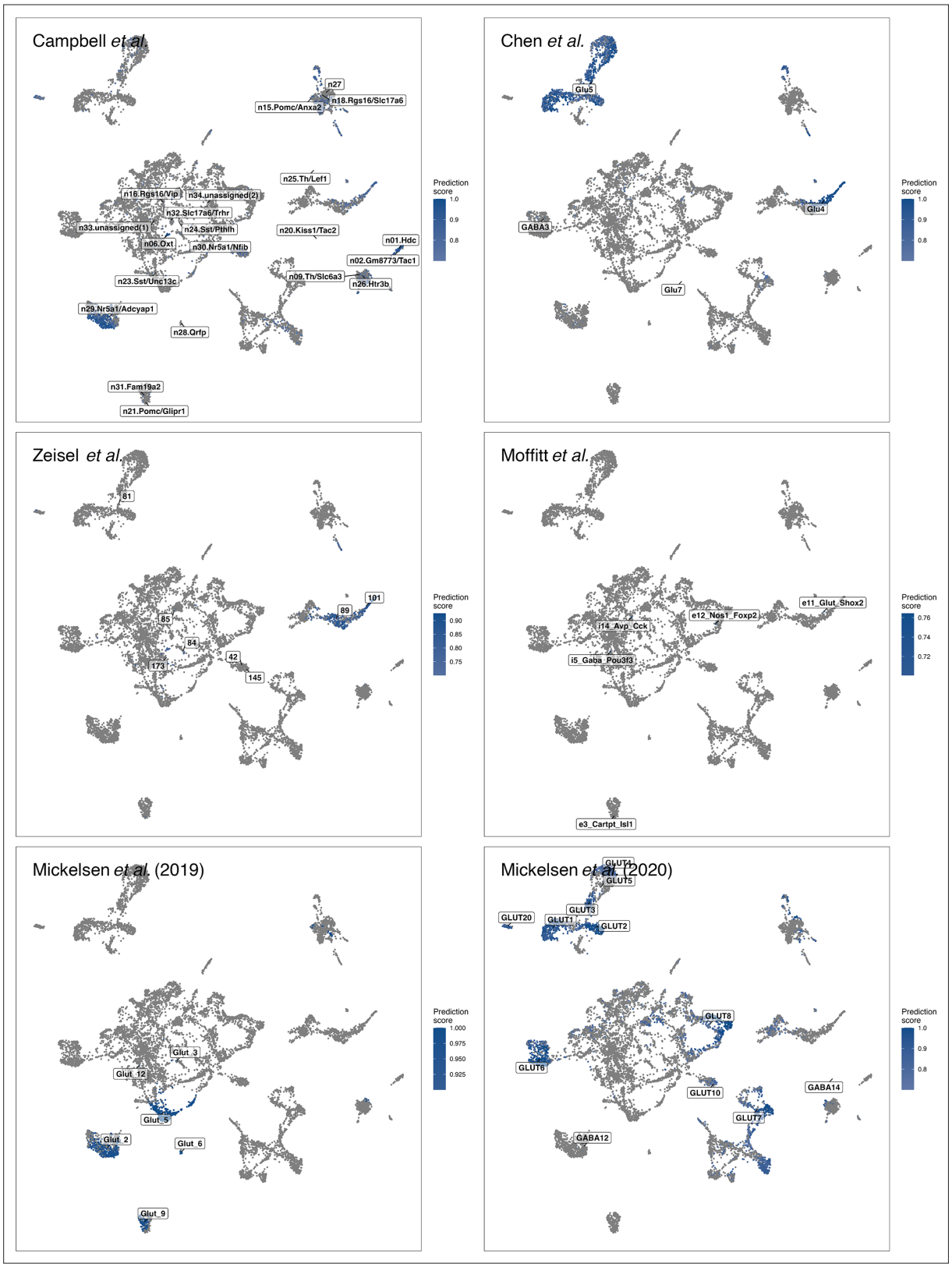

Figure 3—figure supplement 3. Cell-type label transfer for glutamatergic cells. Depicting the prediction scores and potential cell-type labels in glutamatergic cells from different published datasets (***Campbell et al., 2017***; ***Chen et al., 2017***; ***Mickelsen et al., 2019***; ***Mickelsen et al., 2020***; ***Moffitt et al., 2018***; ***Zeisel et al., 2018***).

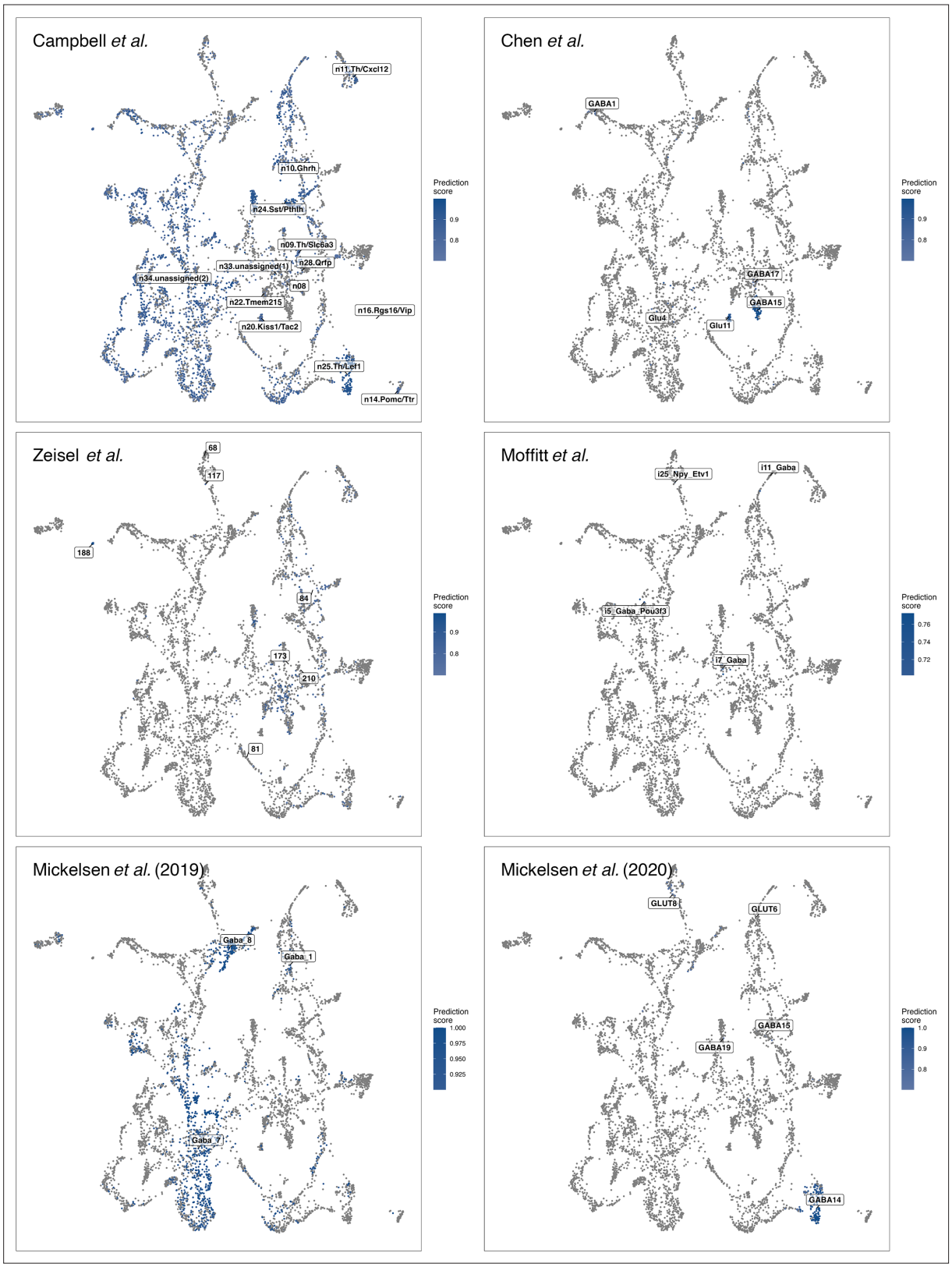

Figure 3—figure supplement 4. Cell-type label transfer for GABAergic cells. Depicting the prediction scores and potential cell-type labels in GABAergic cells from different published datasets (***Campbell et al., 2017***; ***Chen et al., 2017***; ***Mickelsen et al., 2019***; ***Mickelsen et al., 2020***; ***Moffitt et al., 2018***; ***Zeisel et al., 2018***).

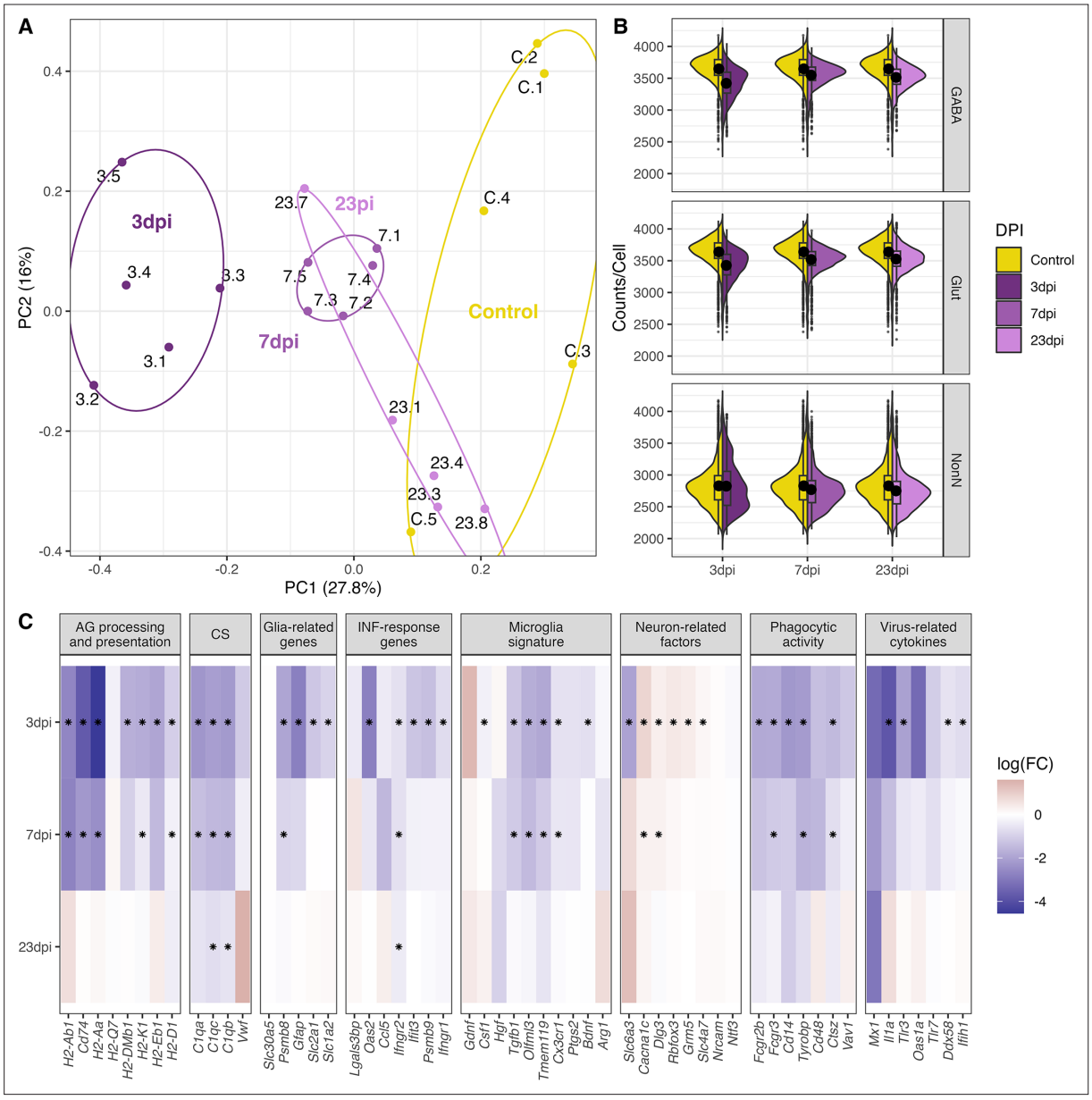

Figure 4. General changes in the transcriptomic landscape of the hypothalamus during peripheral IAV infections. (**A**) Principial component plot of combined counts per sample. Each sample snRNA-library were down-sampled to a total of 300 cells (100 non-neuronal, 100 GABAergic, 100 glutamatergic cells) before normalized counts were aggregated before principal component analysis. Samples are color-coded according to their group membership and the numbers correspond to the individual animal IDs. (**B**) Violin plot showing the distribution of counts per cell at the different time points. The three points of infections are compared to the control group. (**C**) Heatmap showing log-transformed log-fold changes of known immune-related genes. Black stars indicate significant expression (FDR ≤ 0.05).

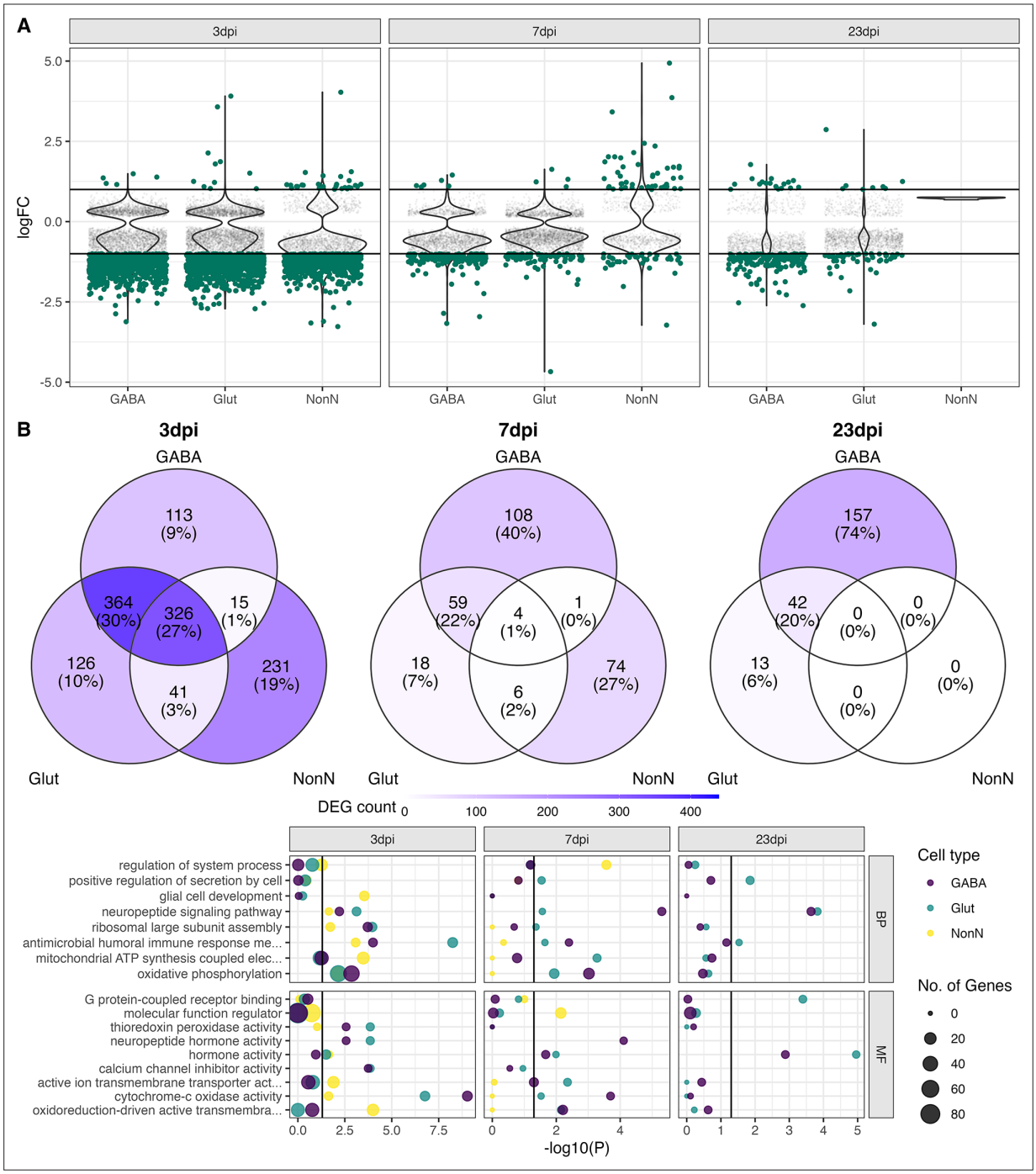

Figure 5. Transcriptional changes in GABAergic and glutamatergic neurons of the hypothalamus during peripheral IAV infections. (**A**.) Violin plots showing the log-transformed fold changes (logFC) per gene calculated for the GABAergic, glutamatergic, and non-neuronal cells at 3, 7, and 23 dpi. Dark-green dots represent significantly differential expressed genes (FDR ≤ 0.05) with a logFC greater than 1 or lower than –1. Small grey dots show significantly expressed genes with a logFC between –1 and 1. (**B**) Venn diagrams depicting the overlap of highly differential expressed genes (logFC >1 or logFC < –1) between the three main cell type clusters at each time point. (**C**) Gene ontology analysis showing the most significant ontology terms for the category of Biological Process (BP, top) and Molecular Function (MF, bottom). The two highest significant ontology's for each time point and each cell type were chosen if it included more than 4 annotated genes. The size of the dots indicates the number of genes included in the ontology term and the colour show the cell type annotation.

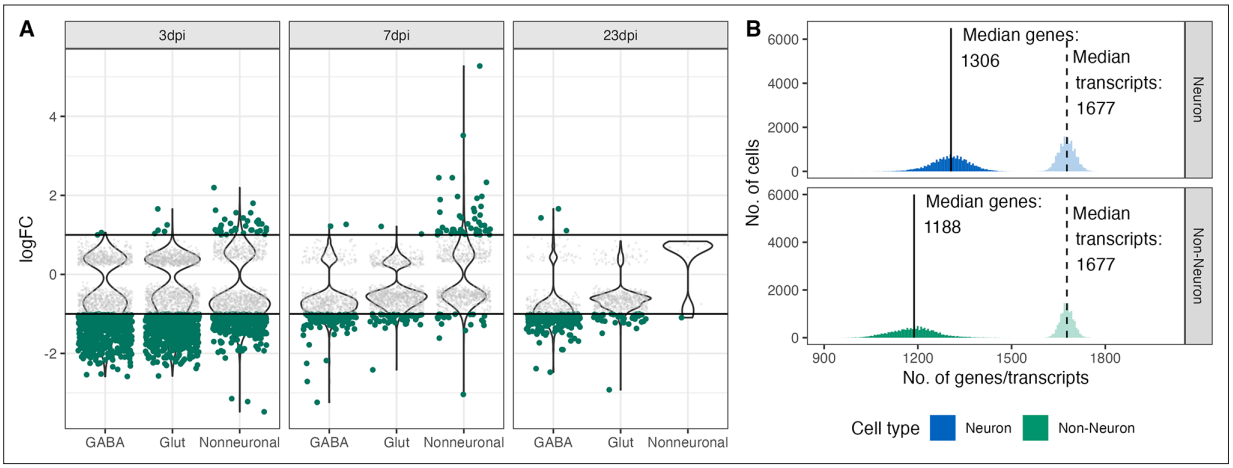

Figure 5—figure supplement 1. DEG analysis in down-sampled dataset. lepsy onset is seasonal and incr(**A**) Scatter- and Violin-plot showing the results of a differential gene expression analysis comparing infected groups against control groups on all Glutamatergic, GABAergic and Non-neuronal cells on a down sampled data set. (**B**) Histogram showing the distribution of features (genes) and transcripts per cell in a down0sampled dataset (down-sampled to 1600 transcripts per cell).

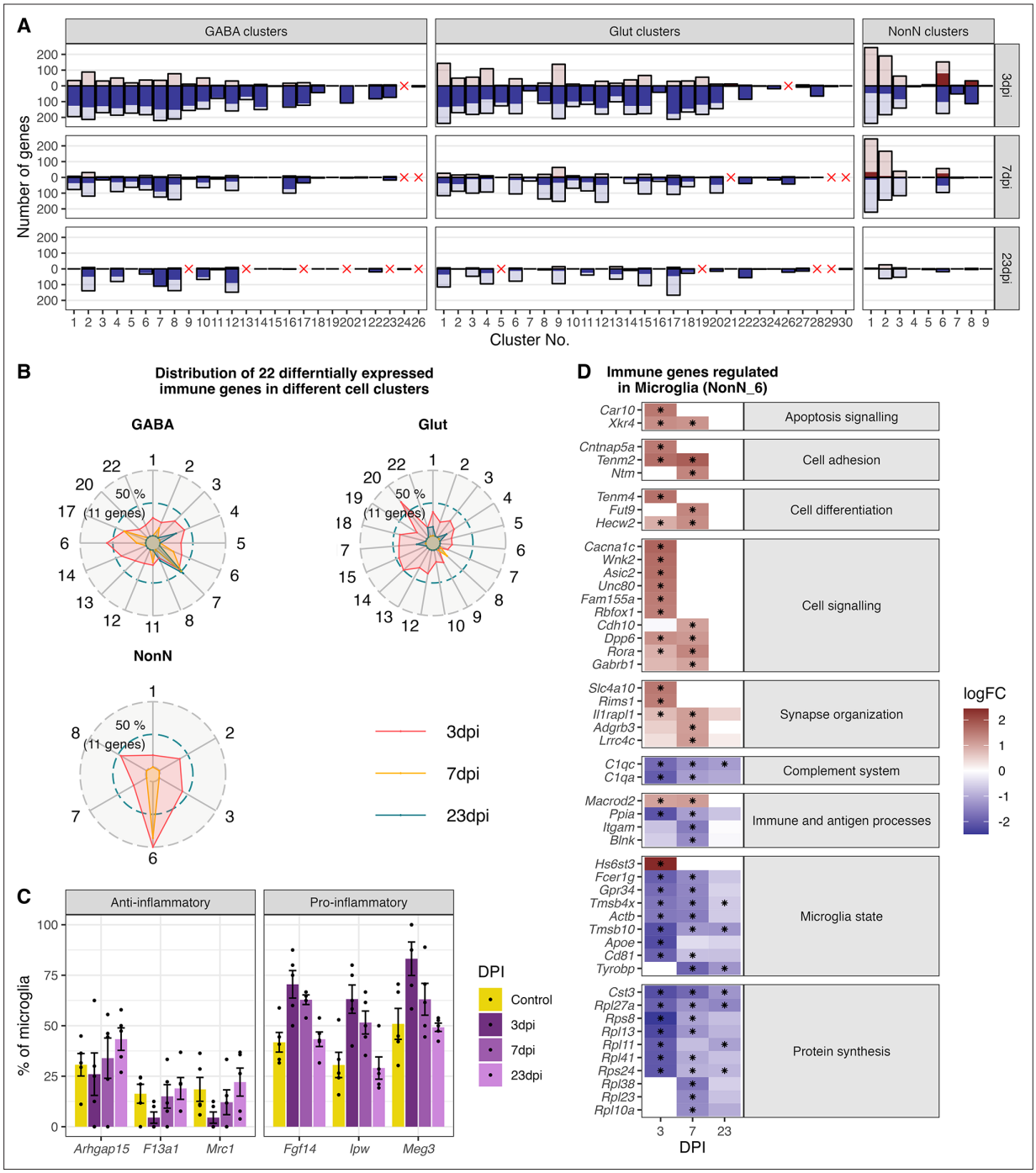

Figure 6. Gene expression changes in different cell type clusters and microglia activation during peripheral IAV infections. (**A**) Bar plot showing the number of significantly differentially expressed genes in each cell type cluster at 3, 7, and 23 dpi. Dark solid blue and red bars show the number of highly differential expressed gene (FDR ≤ 0.05, logFC <= –1 or logFC ≥ 1) per cell type cluster and time point. Lighter shaded bars depict the number of all significant regulated genes (FDR ≤ 0.05, logFC ≥ 0 or logFC ≤ 0). Differentially expressed genes (DEGs) were only included for clusters containing at least three cells per sample and per time point in the cluster. A red cross indicates instances where these criteria were not met. (**B**) Radar plot showing the number of significantly and strongly regulated genes (FDR ≤ 0.05, logFC ≥ 1 or logFC<= –1: n=22) involved in immune processes (based on their gene ontology annotations) per cell cluster at the different time points (red: 3 dpi, yellow: 7 dpi, blue: 23 dpi). (**C**) Percentage of the number of cells expressing distinct anti- or pro-inflammatory signature genes in the microglia cluster. Cells with a raw count of 0 for a gene were assumed as non-expressing, all other cells were assumed to express this gene. Shown are percentages of microglia cells expressing a gene compared to all microglia at each time point across all samples. (**D**) Relative changes in expression levels of disease associated genes within the microglia cluster. Data is show as log-transformed fold changes (logFC) of each time point compared with control group. Black stars depict significant differentially expressed genes (FDR ≤ 0.05).

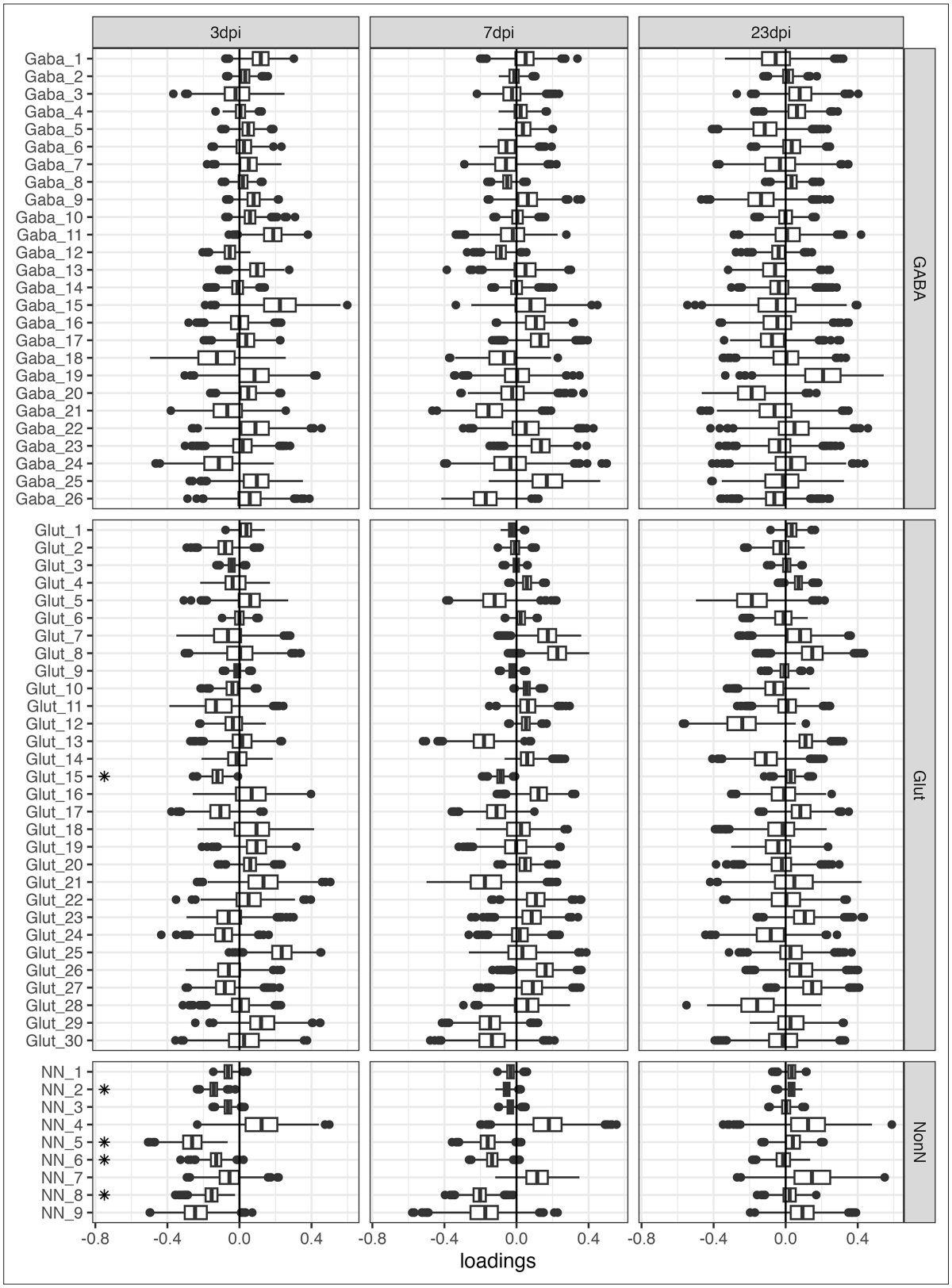

Figure 6—figure supplement 1. Cluster-based composition shifts calculated by Cacoa. Box-plots shwoing cluster-based expression shifts of the different infected groups in comparison to the control calculated with the Cacoa package (***Petukhov et al., 2022***). Shifts on the x-axis in the negative space show a increase of cell proportions in the control samples, whereas a shift towards the positive space indicate an increase in the different infected groups (3, 7, and 23 dpi). Stars depict significance change in cell densities ($p \leq 0.05$ after BH correction).

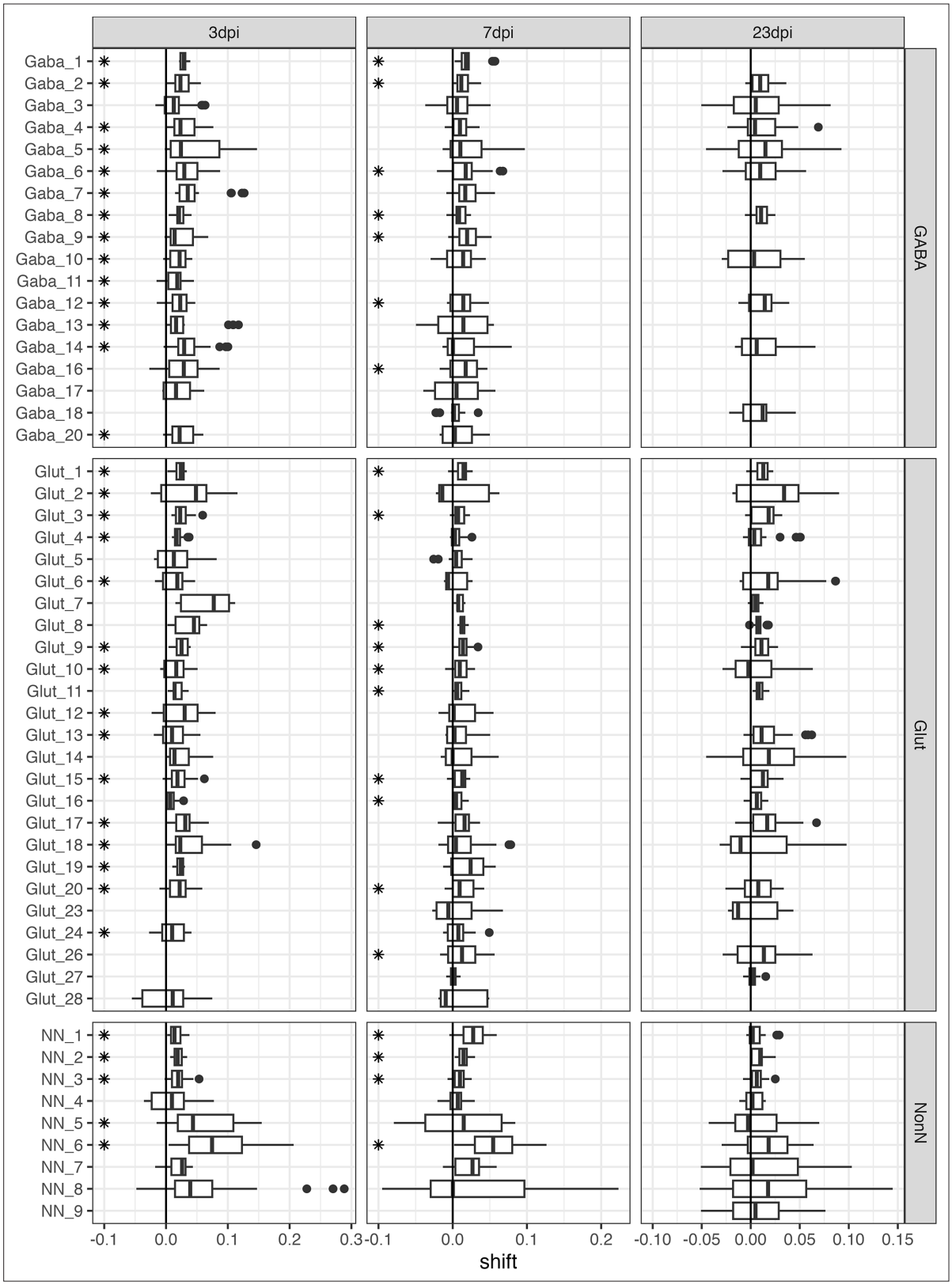

Figure 6—figure supplement 2. Cluster-based analysis of changes in expression magnitudes. Boxplots show the shifts in expression magnitudes based on Cacoa package (***Petukhov et al., 2022***) in the different infected samples compared to the control group. Stars depict a significant change in expression in a cluster ($p \leq 0.05$, after BH correction).

Figure 6—figure supplement 3. Cluster-free expression shifts. UMAP embedding showing of the whole dataset showing adjusted statistical significance levels (color) of expression shift magnitudes. Analysis was performed based on Cacoa package (***Petukhov et al., 2022***).

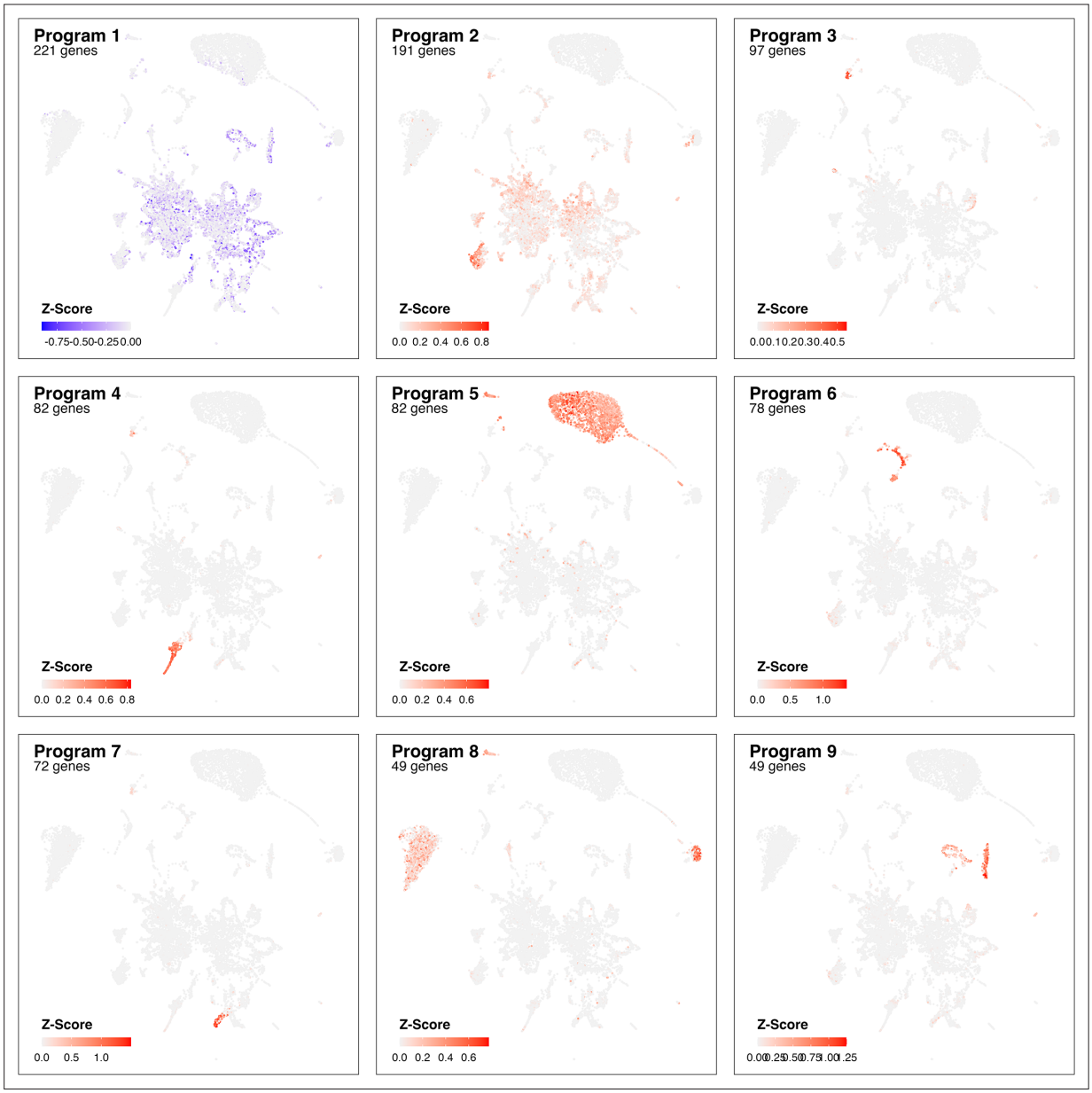

Figure 6—figure supplement 4. Identified gene programs at 3 dpi based on cluster-free genes expression analysis. Adjusted z-scores are shown (color) for most pronounce genes programs identified comparing Control samples with infection at 3 dpi.

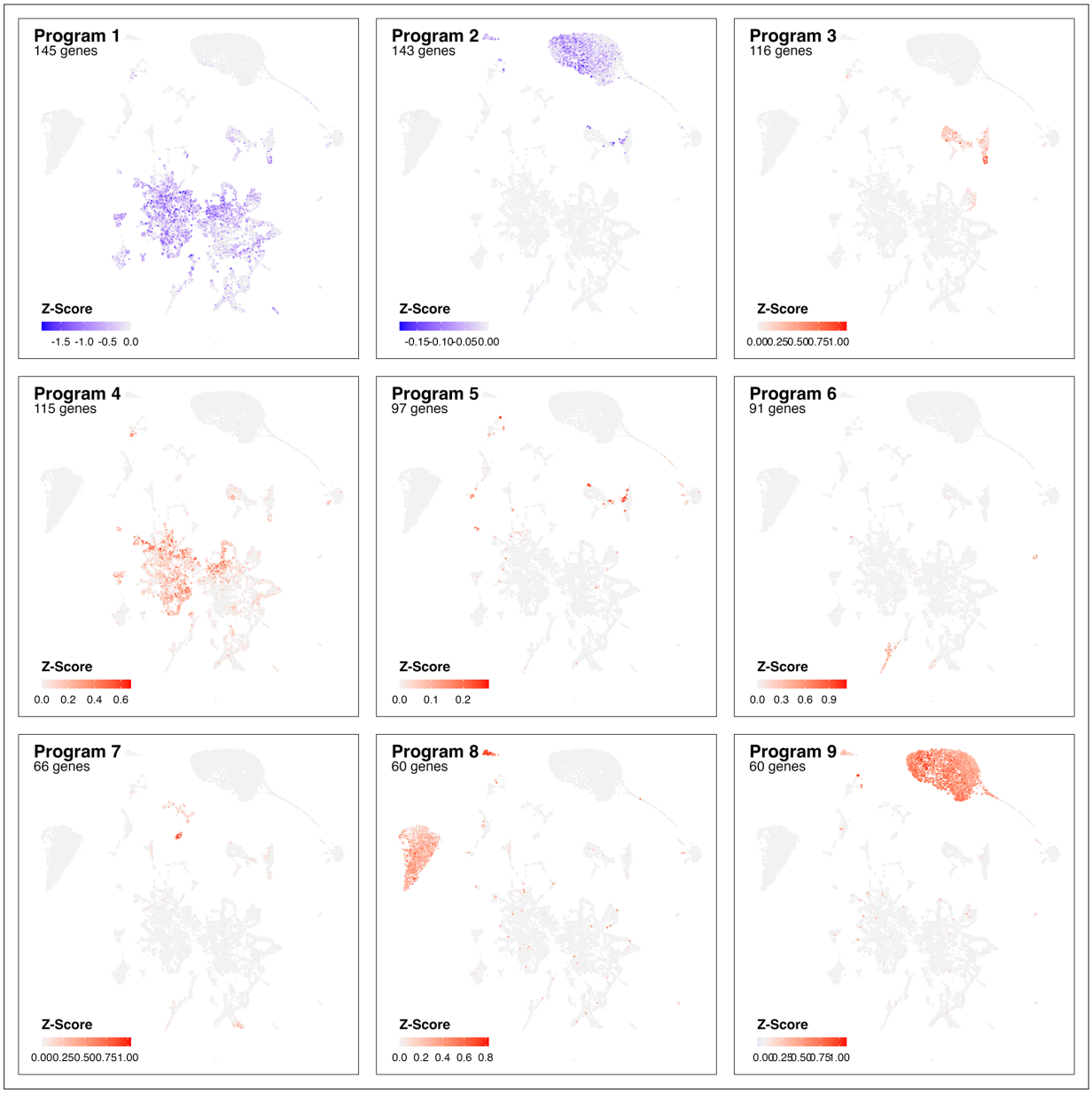

Figure 6—figure supplement 5. Identified gene programs at 3 dpi based on cluster-free genes expression analysis. Adjusted z-scores are shown (color) for most pronounce genes programs identified comparing Control samples with infection at 7 dpi.

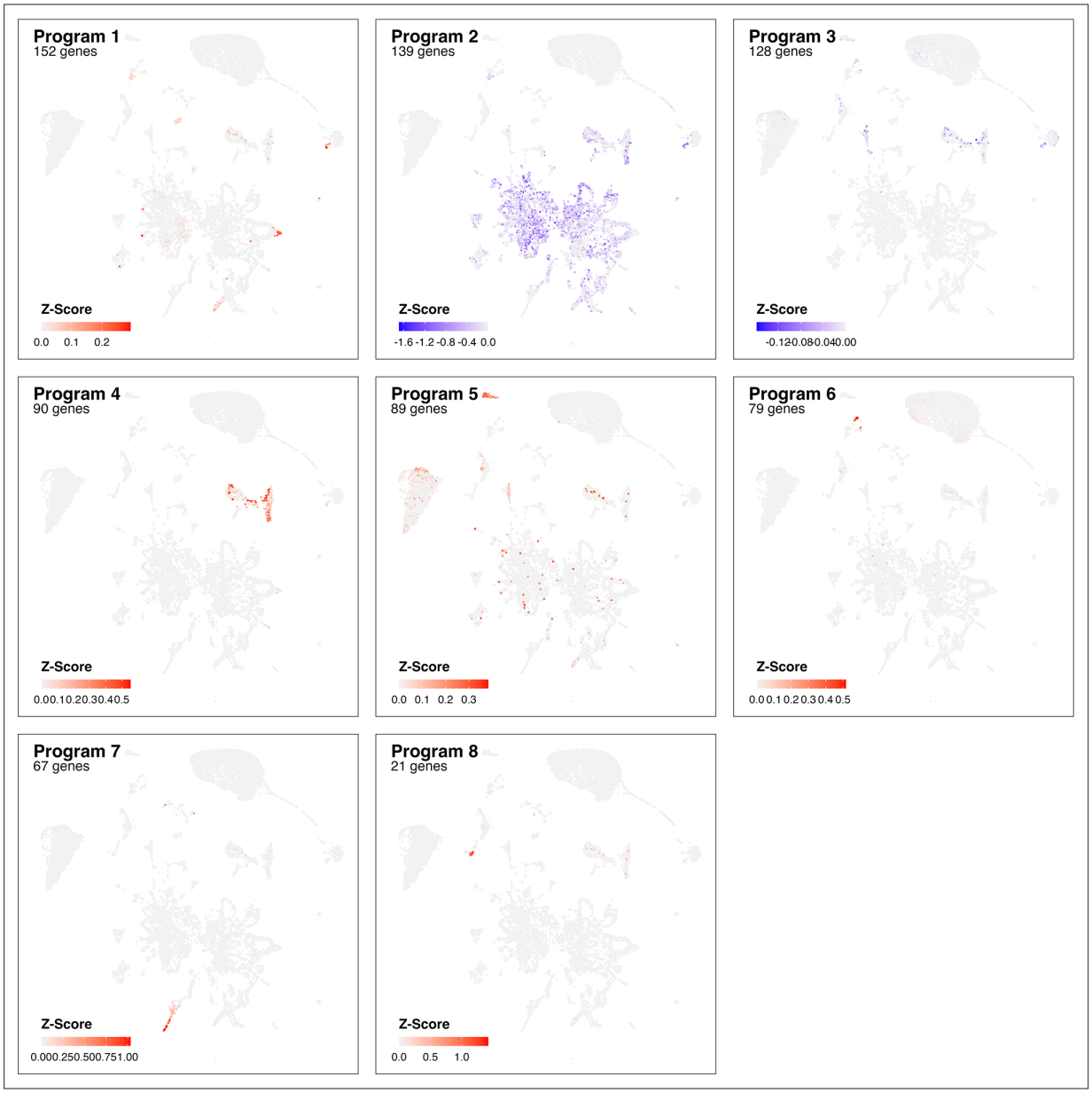

Figure 6—figure supplement 6. Identified gene programs at 3 dpi based on cluster-free genes expression analysis. Adjusted z-scores are shown (color) for most pronounce genes programs identified comparing Control samples with infection at 23 dpi.

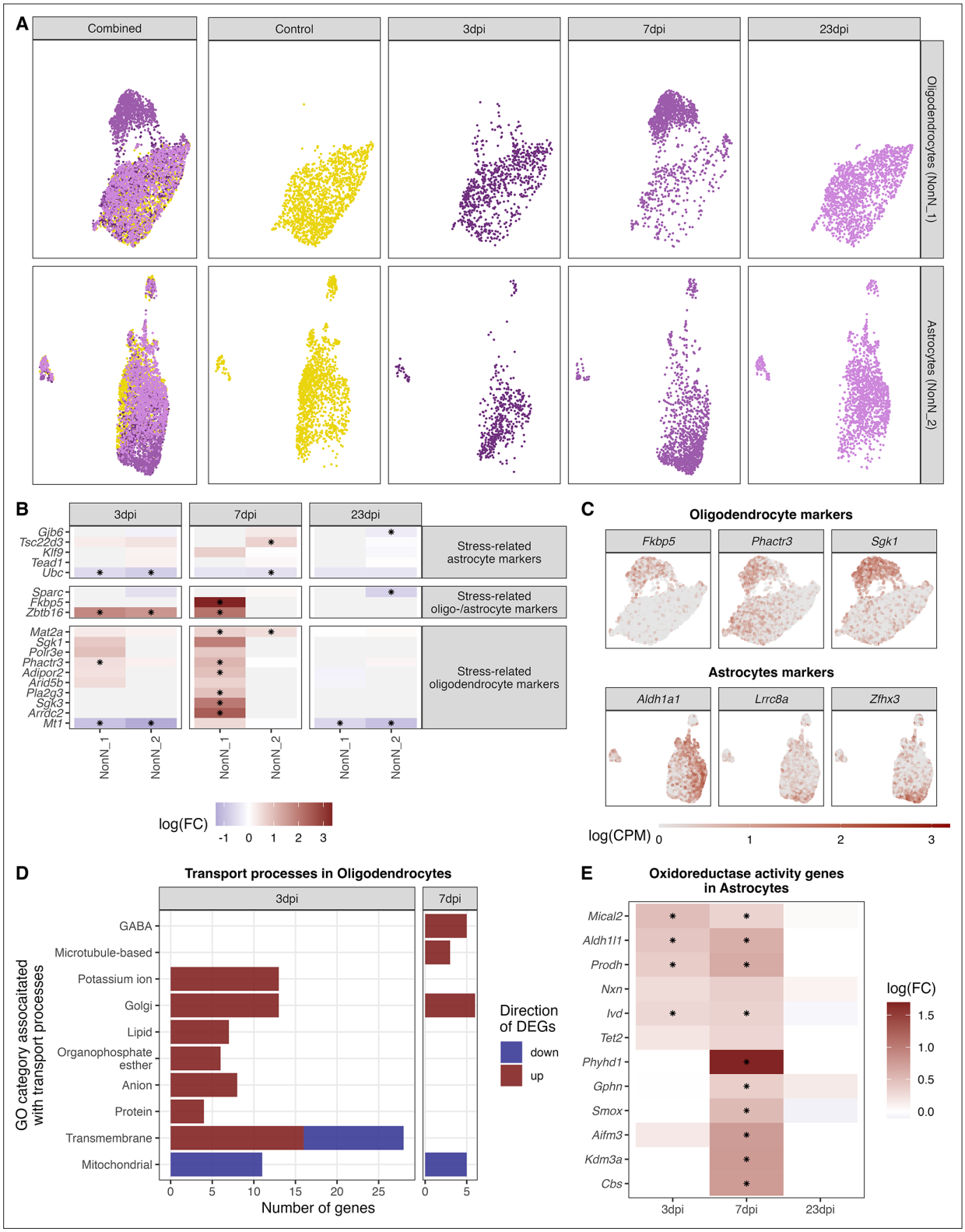

Figure 7. Identification of distinct oligodendrocyte and astrocyte sub-clusters at 7 dpi. (**A**) Combined UMAP plot of all cells of the oligodendrocyte (upper right, n=5.023) and astrocyte (lower right, n=4.542) cluster in controls and at different time points. (**B**) Relative gene expression changes (in comparison of to the mock-infected group) of stress-related oligodendrocyte and astrocyte markers within the oligodendrocyte (NN_1) and astrocyte (NN_2) subcluster. Data is shown as log-transformed fold changes, an asterisks indicates statistical significance (FDR ≤ 0.05). (**C**) Normalized expression values of selected marker genes at 7-dpi in UMAP plots of all oligodendrocytes or astrocytes. (**D**) Number of differentially expressed genes (FDR ≤

Figure 7 continued on next page

Figure 7 continued

0.05, logFC <= –1 or logFC ≥ 1) annotated to gene ontologies associated with transport process in the oligodendrocytes at 3 and 7 dpi. (**E**) Expression dynamics of differential expressed oxidoreductase genes in the astrocyte cluster at 3, 7, and 23 dpi. A black star indicated significant differential expression (FDR ≤ 0.05).

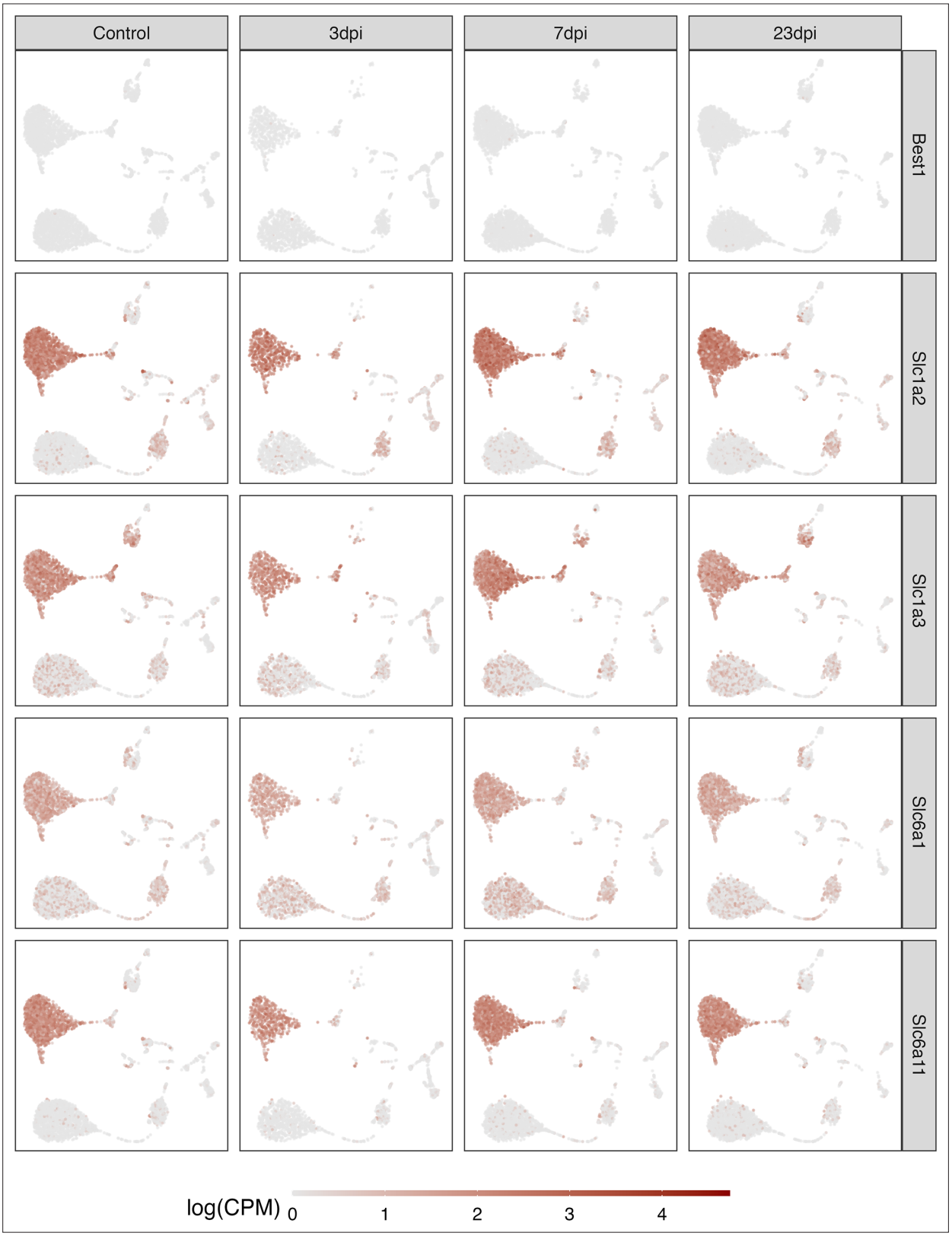

Figure 7—figure supplement 1. Expression of different GABAergic and glutamatergic transporters. Depicted are normalized expression levels in non-neuronal cells of different GABAergic and glutamatergic transporters.

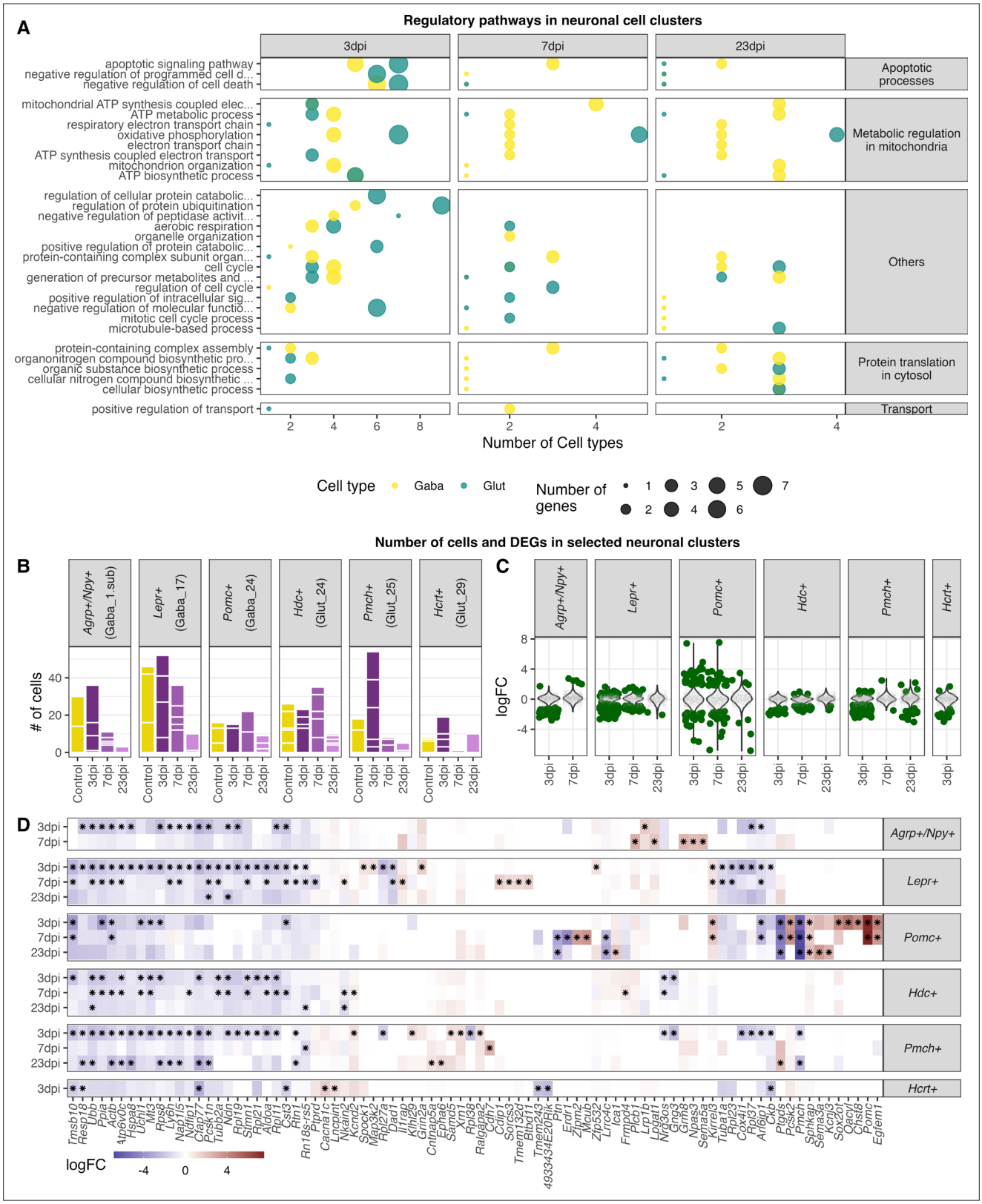

Figure 8. Highly enriched gene ontology categories in neuronal cell populations at different time points of infections. (**A**) Dot-plot depicting the number of neuronal cell populations significantly enriched gene ontology categories. Only cell clusters with at least 10 significantly differently expressed genes (logFC <= –1 or logFC ≥ 1, FDR≤ 1) in all three analysed time points were included in the here presented plot. Neuronal cell clusters included are (GABA_2, 4, 6, 8, 10,12; Glut_1, 3, 4, 6, 9, 11, 13, 15, 17). Only significantly enriched (*Pelim* ≤ 0.05) gene ontology terms were chosen and for each

Figure 8 continued on next page

Figure 8 continued

cluster per time point the 10 most enriched GO terms were included. (**B**) Bar plot depicting the amount of captured nuclei in the individual animals at the different time points for known hypothalamic neuron populations. (**C**) Differential expressed genes in selected neuron populations. Dark green dots show significantly differential expressed genes (FDR ≤ 0.05). (**D**) Heatmap showing the five highest and lowest DEGs (FDR ≤ 0.05) in each neuronal population.

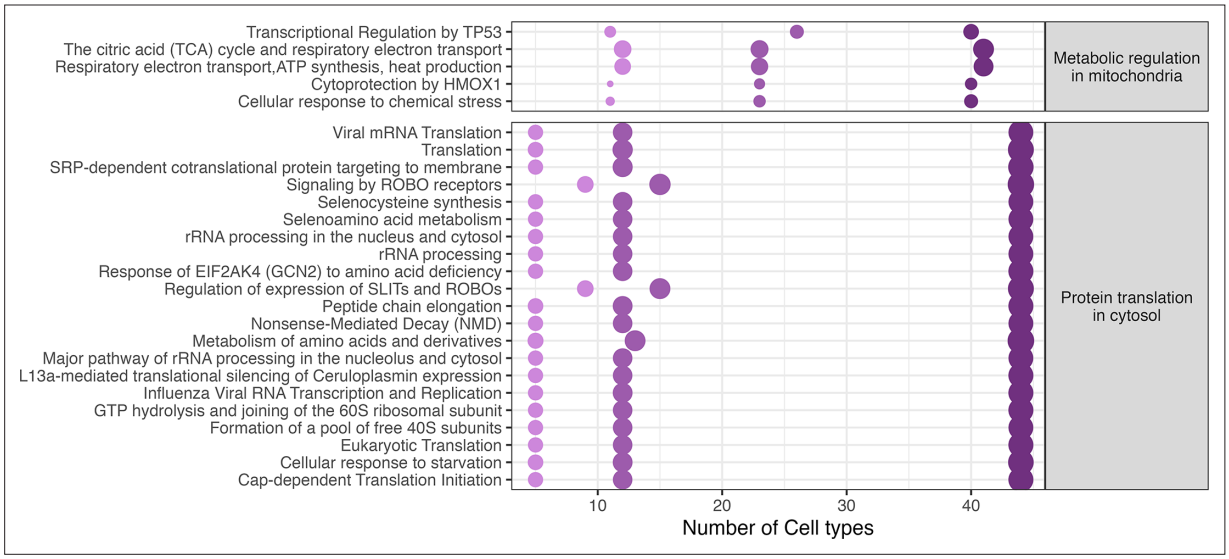

Figure 8—figure supplement 1. Reactome pathway enrichment of differentially expressed genes in neurons. Dotplot shows significantly enriched Reachtome pathways in neuronal cell popluations across different timepoints. Gradients of purple depict reflect the time points of analysis. 3 dpi (dark purple) to 23dpi (light purple).

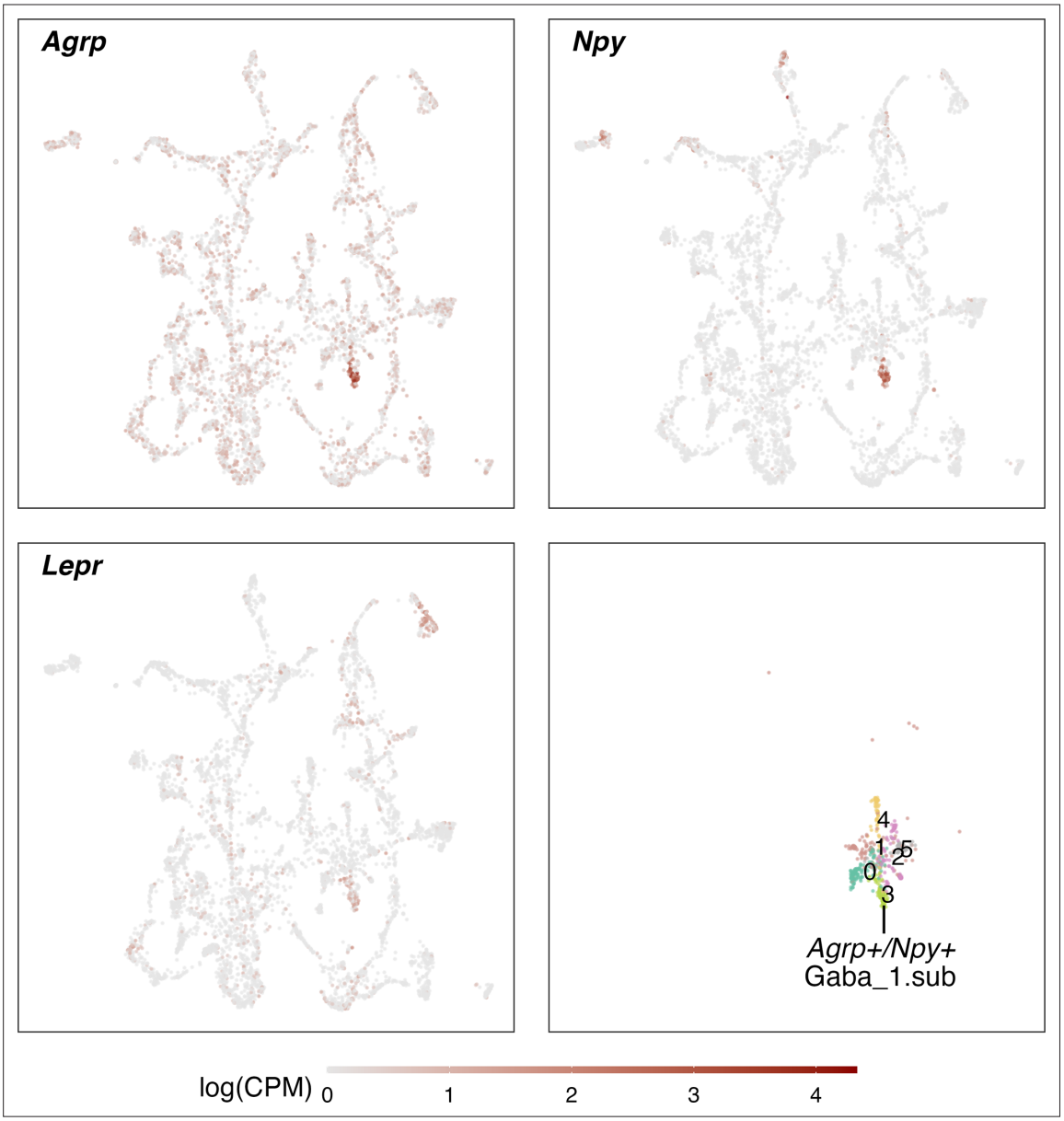

Figure 8—figure supplement 2. Identification of an *Agrp*+/Npy +neuron cluster. *Agrp*+/Npy +neurons were identified as a subcluster of the GABA_1 neuron population. Depicted are the normalized expression levels of marker genes *Agrp*, *Npy* and *Lepr*, showing their distinct expression in a cell cluster within the GABA_1 cluster. An additional cluster analysis of the GABA_1 cluster, identified them in the subcluster 3 (lower left).

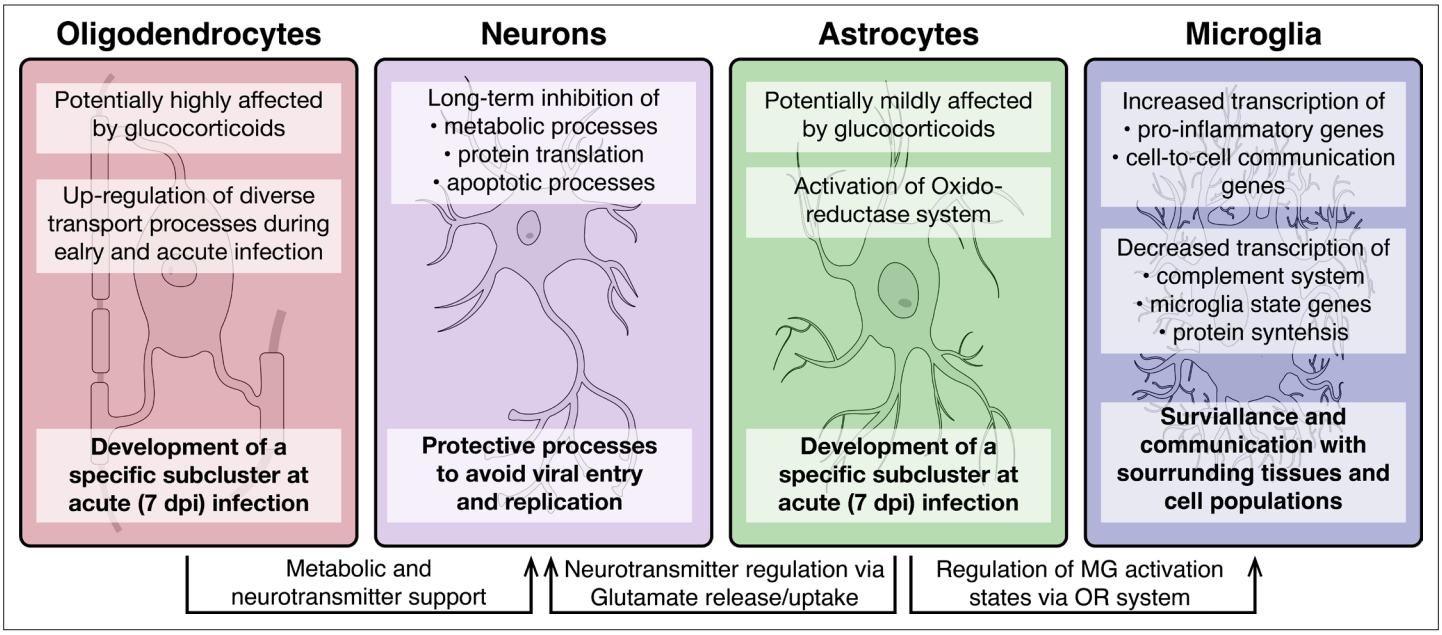

Figure 9. Overview of molecular processes occurring in different cell types within the hypothalamus during a peripheral H1N1 IAV infection. Schematic overview of the main molecular mechanisms of oligodendrocytes, astrocytes, microglia and neurons during acute to late immune responses of a peripheral IAV infection with the H1N1 pdm09 Influenza A virus.